Journal of Medicinal Chemistry

Article

pubs.acs.org/jmc

Novel Substituted Benzothiophene and Thienothiophene Carboxanilides and Quinolones: Synthesis, Photochemical Synthesis, DNA-Binding Properties, Antitumor Evaluation and 3D-Derived QSAR Analysis

Maja Aleksić,[†] Branimir Bertoša,[‡] Raja Nhili,[⊥] Lidija Uzelac,[§] Ivana Jarak,[†,#] Sabine Depauw,[⊥] Marie-Hélène David-Cordonnier,[⊥] Marijeta Kralj,[§] Sanja Tomić,*[,‡] and Grace Karminski-Zamola*[,†]

[†]Department of Organic Chemistry, Faculty of Chemical Engineering and Technology, University of Zagreb, Marulićev trg 20, P.O. Box 177, HR-10000 Zagreb, Croatia

[‡]Division of Physical Chemistry and [§]Division of Molecular Medicine, "Ruđer Bošković" Institute, Bijenička cesta 54, P.O. Box 1016, HR-10000 Zagreb, Croatia

[⊥]INSERM U837-JPARC (Jean-Pierre Aubert Research Center), Team "Molecular and Cellular Targeting for Cancer Treatment", Université Lille Nord de France, IFR-114, Institut pour la Recherche sur le Cancer de Lille, Place de Verdun, F-59045 Lille Cedex, France

Supporting Information

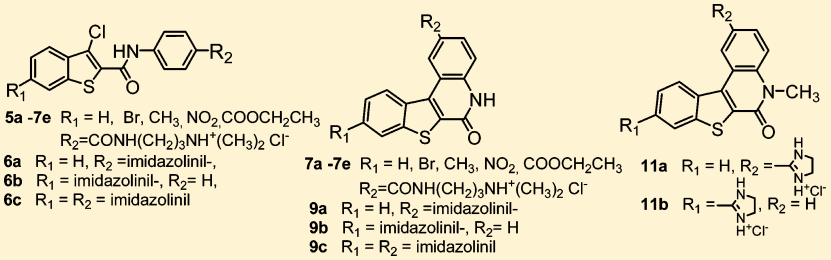

ABSTRACT: A series of new *N*,*N*-dimethylaminopropyl- and 2-imidazolinyl-substituted derivatives of benzo[*b*]thienyl- and thieno[2,3-*b*]thienylcarboxanilides and benzo[*b*]thieno[2,3-*c*]- and thieno[3′,2′:4,5]thieno[2,3-*c*]quinolones were prepared. Quinolones were prepared by the reaction of photochemical dehydrohalogenation of corresponding anilides. Carboxanilides and quinolones were tested for the antiproliferative activity. 2-Imidazolinyl-substituted derivatives showed very prominent activity. By use of the experimentally obtained antitumor measurements, 3D-derived QSAR analysis was performed for the set of compounds. Higly predicitive 3D-derived QSAR models were obtained, and molecular properties that have the highest impact on antitumor activity were identified. Carboxanilides **6a**−**c** and quinolones **9a**−**c** and **11a** were evaluated for DNA binding propensities and topoisomerases I and II inhibition as part of their mechanism of action assessment. The evaluated differences in the mode of action nicely correlate with the results of the 3D-QSAR analysis. Taken together, the results indicate which modifications of the compounds from the series should further improve their anticancer properties.

INTRODUCTION

Substituted heterocyclic quinolones exhibit several pharmacological activities and have therefore attracted considerable attention from medicinal and synthetic organic chemists.[1−4] As a part of our continuing search for potential anticancer agents related to heterocyclic quinolones, we have previously reported synthesis and strong inhibitory activities on several human tumor cell lines of thieno[3′,2′:4,5]thieno- and benzo[*b*]thieno-[2,3-*c*]quinolones, containing a *N*,*N*-dimethylaminopropyl substituent in the amide part of the molecule and on the quinolone nitrogen (Figure 1).[5,6] Moreover, we also reported the synthesis and antiproliferative activity of various cyano- and/or amidino-substituted benzo[*b*]thieno[2,3-*c*]quionolones and their acyclic precursors,[7] since it is well-known that amidines are structural parts of numerous compounds of biological interest as various medical and biochemical agents. Amidino-substituted benzo[*b*]thieno[2,3-*c*]quinolones, strong ds-DNA/RNA intercalators, showed in general stronger and more selective antitumor activity than acyclic precursors, which did not intercalate at all. Compounds with one amidino group as substituent have shown the best antiproliferative effect on the cell lines tested. This could be explained by the permanent positive charge placed on the amidino group, which may start a number of additional interactions. Unexpectedly, the introduction of two amidino groups diminished the biological activity, possibly because of steric effects. To elucidate the impact of variation of thiophene vs benzene ring, we have also prepared

Received: December 13, 2011
Published: May 24, 2012

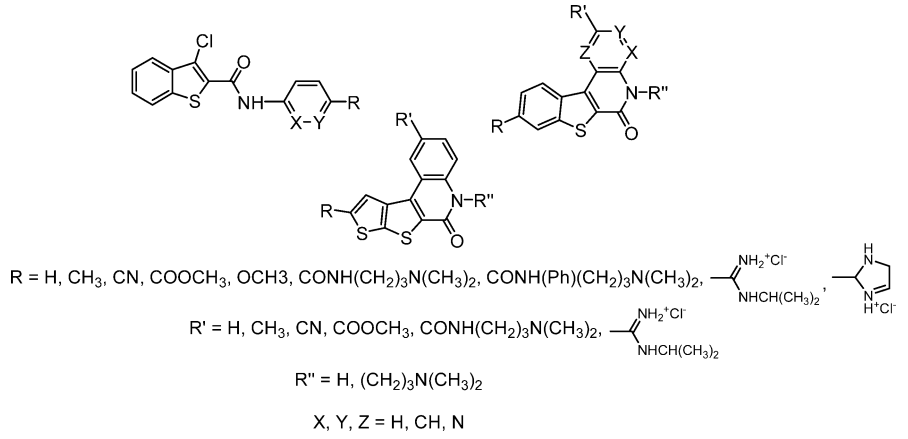

Figure 1. Structures of earlier prepared carboxamides, quinolones, and naphthyridones.[5,6]

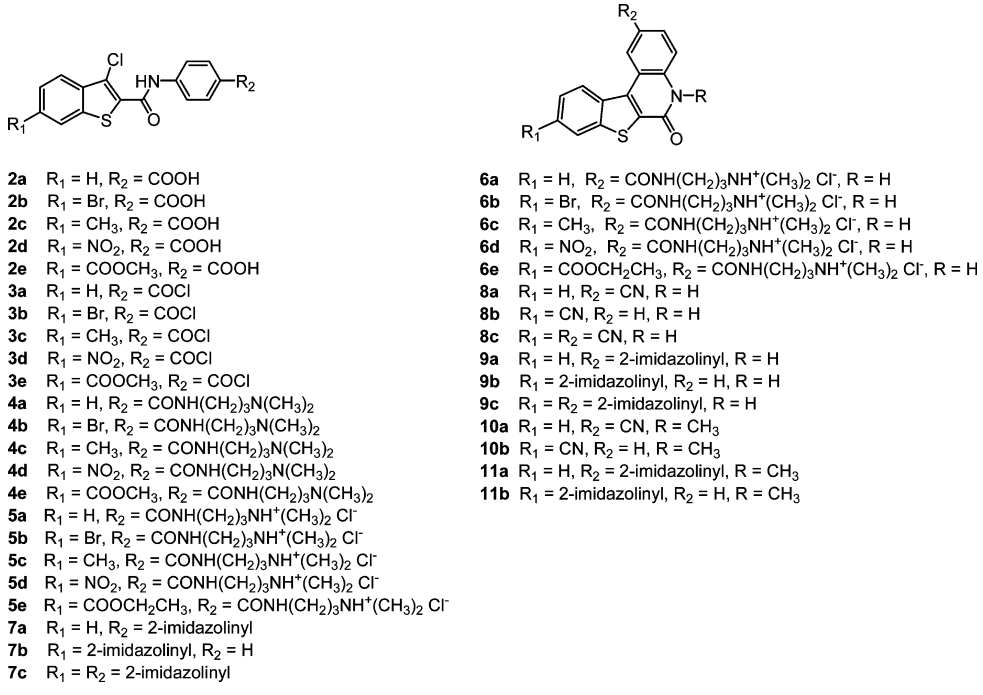

Figure 2. Substituted 3-chlorobenzo[*b*]thiophene-2-carboxamides and benzo[*b*]thieno[2,3-*c*]quinolones.

amidino-substituted thieno[3′,2′:4,5]thieno- and thieno-[2′,3′:4,5]thieno[2,3-*c*]quinolones as well as their acyclic precursors, whereby both cyclic and acyclic compounds showed pronounced antitumor activity.[8] Replacement of the benzene ring with pyridine, in the amino part of the amides and naphthyridones, and the acyclic amidino groups with cyclic amidino 2-imidazolinyl group resulted in an increase of the antitumor activity. Some of the naphthyridone compounds were active in the submicromolar range, with special selectivity to MiaPaCa-2[a], HeLa, and SW620 cells. The most promising compounds inhibited tumor growth and topoisomerase activity, which was related to their high DNA binding capacity, whereby the 2-imidazolinyl-substituted derivatives showed the most prominent activity.[9] All of the above-mentioned considerations prompted us to prepare novel *N*,*N*-dimethylaminopropyl- and 2-imidazolinyl-substituted derivatives of benzo[*b*]thieno-, thieno[3′,2′:4,5]thieno-, and thieno[2′,3′:4,5]thieno[2,3-*c*]-quinolones (Figures 2 and 3).

In order to identify molecular properties that have the largest impact on antitumor activity of the investigated compounds, we

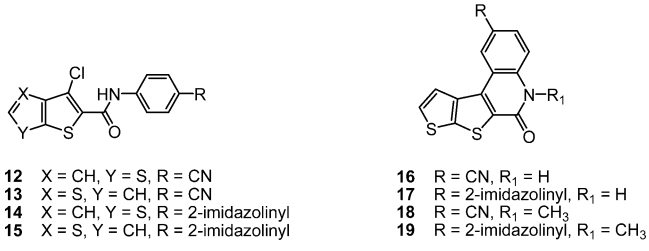

Figure 3. Substituted 3-chlorothieno[2,3-*b*]- and 3-chlorothieno[3,2-*b*]thiophene-2-carboxamides and thieno[3′,2′:4,5]thieno- and thieno-[2′,3′:4,5]thieno[2,3-*c*]quinolones.

performed the 3D-derived QSAR analysis using the Volsurf based procedure. The main advantage of this approach is usage of descriptors that have clear chemical or physical meaning and are independent of the molecular superposition. Besides structural properties, VolSurf+ descriptors describe the ADME (absorption, distribution, metabolism, and excretion) properties of the molecule as well. Similar approaches for

dx.doi.org/10.1021/jm300505h | *J. Med. Chem.* 2012, 55, 5044−5060

Scheme 1. Synthesis of 3-Chlorobenzo[*b*]thiophene-2-carboxamides and Benzo[*b*]thieno[2,3-*c*]quinolones

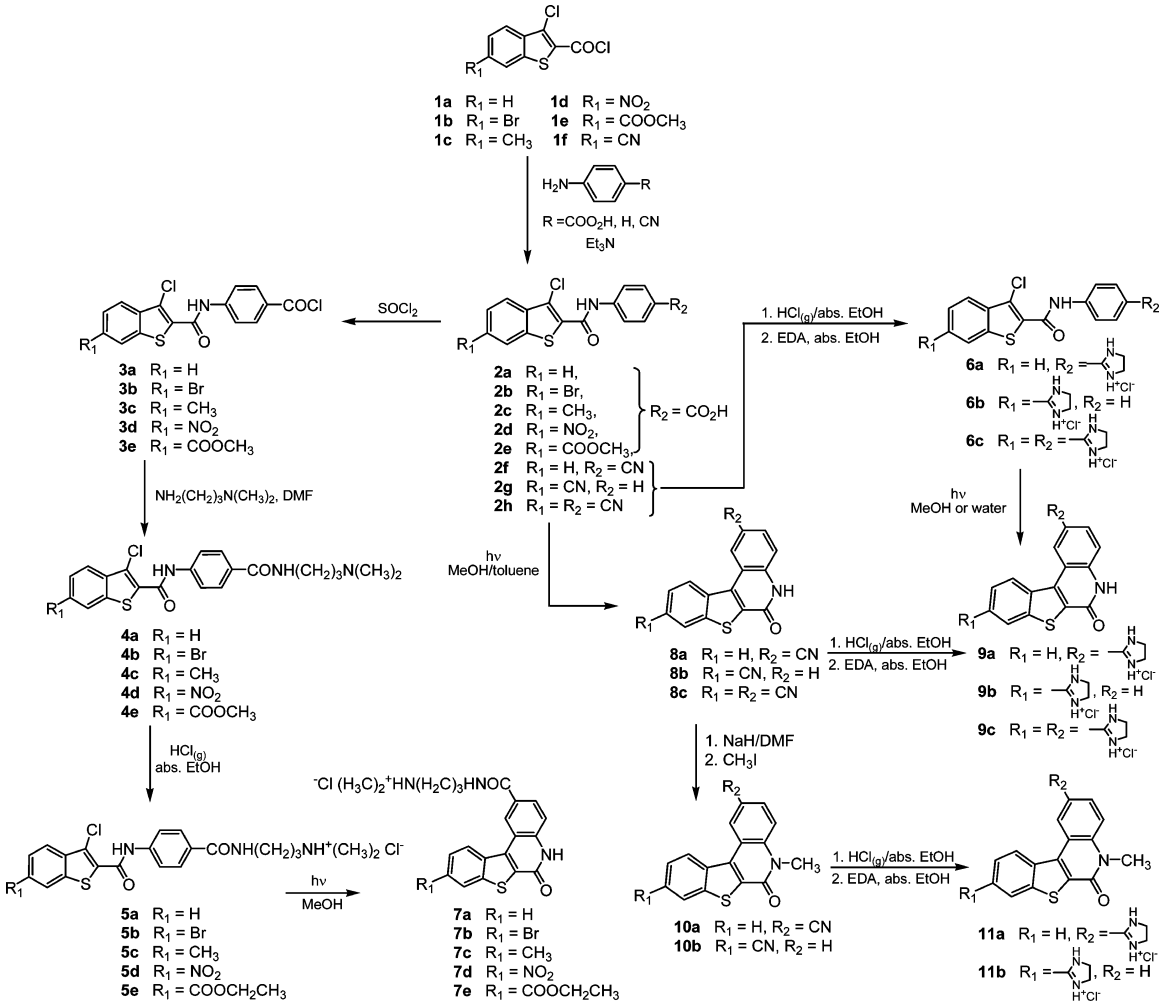

building 3D-derived QSAR models have already been proven to be successful and useful in investigation of different classes of the potentially biologically active compounds.[10−12]

RESULTS AND DISCUSSION

Chemistry. All compounds (**2a−19**) shown in Figures 2 and 3 were prepared according to the Schemes 1 and 2, starting from substituted 3-chlorobenzo[*b*]thiophenecarbonyl chlorides (**1a−f**)[6] and 3-chlorothieno[2,3-*b*]thiophene- or 3-chloro[3,2-*b*]thiophene-2-carbonyl chlorides.[8] Chlorides **1a−e** gave in the reaction with *p*-aminobenzoic acid 6-substituted *N*-(4-carboxyphenyl)-3-chlorobenzo[*b*]thiophene-2-carboxamides **2a−e**, which in the reaction with $SOCl_2$ gave corresponding acid chlorides 6-substituted *N*-(4-chlorocarbonylphenyl)-3-chlorobenzo[*b*]thiophene-2-carboxamides **3a−e**. 6-Substituted 2-{*N*-[4-*N*-(3-dimethylamino)propyl]carbamoyl}-3-chlorobenzo[*b*]thiophene anilides **4a−e** were prepared from **3a−e** in the reaction with *N*,*N*-dimethylaminopropylamine. The formation of the new amide bond was supported by the appearance of a new triplet peak at approximately 8.5 ppm in the ^{1}H NMR spectra of compounds **4a−e**. The hydrochloride salts of *N*,*N*-dimethylaminopropyl-substituted carboxamides **5a−e** were prepared by protonation **4a−e** with the saturated ethanolic or methanolic solutions of gaseous HCl. Protonation of tertiary amino nitrogen resulted in the appearance of a broad singlet at around 10 ppm in the ^{1}H NMR spectra of compounds **5a−e**. Since the protonation of compound **4e** was conducted in ethanol, a transesterification reaction gave rise to the corresponding ethylated ester **5e**, which was confirmed by the disappearance of the methyl at the position of 3.93 ppm in the ^{1}H NMR spectra of compound **4e** and the appearance of a quadruplet at 4.35 ppm and a triplet 1.33 ppm, correspondingly, in the ^{1}H NMR spectra of the compound **5e**. Carboxanilides **5a−e** were photochemically transformed into 9-substituted 2-[*N*-3-(dimethylamino)propyl]carbamoyl-6-oxo-5,6-dihydrobenzothieno[2,3-*c*]quinoline hydrochlorides **7a−e** in methanol. Acid chlorides **1a** and **1f** reacted with *p*-aminobenzonitrile to give the corresponding cyano-substituted carboxamides **2f−h**.[7] Cyano-substituted carboxamides **2f−h** were, in the Pinner reaction, transformed into corresponding 2-imidazolinyl-substituted carboxamides **6a−c**. The cyano-substituted carboxamides **2f−h** were photochemically converted in MeOH/toluene medium into cyclic benzo[*b*]thieno[2,3-*c*]-quinolones **8a−c** in yields of 61−92.5%, while 2-imdazolinyl-substituted carboxamide hydrochloride salts **6a−c** were photochemically converted into the corresponding benzo[*b*]thieno-[2,3-*c*]quinolone hydrochloride salts **9a−c**.

The photochemical dehydrohalogenation reaction of compounds **6a** and **6c** was conducted in water to obtain **9a** and **9c** with yields of 32.4−96.4%. The Pinner reaction of cyano-substituted quinolone **8a** gave **9a** with 77% yields, but in the

dx.doi.org/10.1021/jm300505h | *J. Med. Chem.* 2012, 55, 5044−5060

Scheme 2. Synthesis of 3-Chlorothieno[2,3-*b*]- and 3-Chlorothieno[3,2-*b*]thiophene-2-carboxamides and Thieno[3′,2′:4,5]thieno- and Thieno[2′,3′:4,5]thieno[2,3-*c*]quinolones

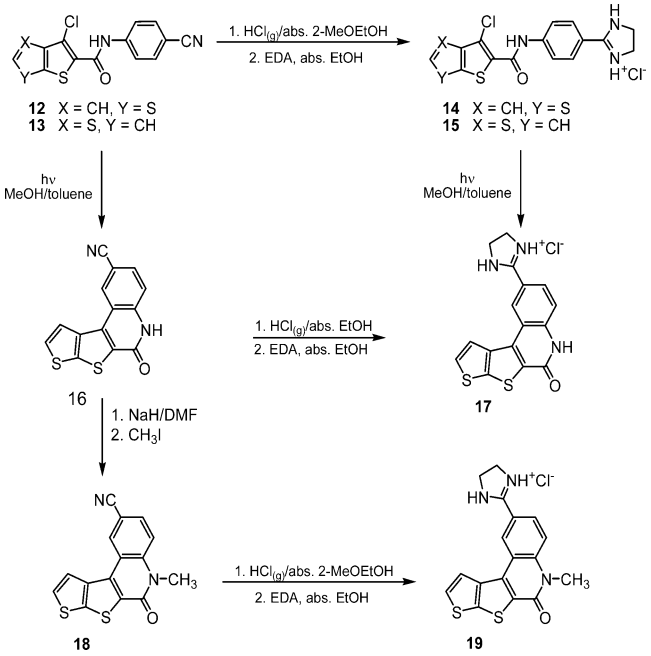

cases of **8b** and **8c** into **9b** and **9c**, the reaction was not successful.

Cyano-substituted quinolones **8a** and **8b** were N-methylated with methyl iodide in the presence of NaH to obtain N-methylated quinolones **10a** and **10b**, which gave in the Pinner reaction 2-(imidazolin-2-yl)-5-methyl-6-oxo-5,6-dihydro[1]-benzothieno[2,3-*c*]quinolin-6-one hydrochloride **11a** and 5-methyl-9-(imidazolin-2-yl)-6-oxo-5,6-dihydro[1]benzothieno-[2,3-*c*]quinolin-6-one dihydrochloride **11b** with yields of 43.9% and 55.5%.

N-(4′-Cyanophenyl)-3-chlorothieno[3,2-*b*]thiophene carboxanilide **12** and *N*-(4′-cyanophenyl)-3-chlorothieno[2,3-*b*]-thiophene carboxanilide **13** (Scheme 2) were prepared from the earlier described 3-chlorothieno[3,2-*b*]thiophene-2-carbonyl chloride or 3-chlorothieno[2,3-*b*]thiophene-2-carbonyl chloride[8] and 4-aminobenzonitrile. In the Pinner reaction, they were converted into the corresponding 2-imdazolinyl-substituted carboxanilides, *N*-[4′-(2-imidazolinyl)phenyl]-3-chlorothieno[3,2-*b*]thiophene carboxanilide **14** and *N*-[4′-(2-imidazolinyl)phenyl]-3-chlorothieno[2,3-*b*]thiophene carboxanilide **15**, as hydrochloride salts. Carboxanilide **12** was photochemically cyclized in methanol/toluene medium into 2-cyano-6-oxo-5,6-dihydrothieno[3′,2′:4,5]thieno[2,3-*c*]-quinoline **16** with a yield of 85% which, after Pinner reaction, gave 2-(2-imidazolinyl)-6-oxo-5,6-dihydrothieno[3′,2′:4,5]-thieno[2,3-*c*]quinoline hydrochloride salt **17** in a yield of 56.9%. The same quinolone **17** was obtained from carboxanilide **14** in a photochemical dehydrohalogenation reaction in MeOH with a yield of 39.1%. Cyano-substituted quinolone **16** was N-methylated into quinolone **18**, which after the Pinner reaction gave 2-(2-imidazolinyl)-5-methy-6-oxo-5,6-dihydrothieno[3′,2′:4,5]thieno[2,3-*c*]quinoline **19** in a yield of 65.1%. All 2-imidazolinyl-substituted carboxanilides, as well as quinolones, show characteristic peaks in ^{1}H NMR spectra for NH and NH protonated 2-imidazolinyl group at about 10−10.9 ppm.

Antiproliferative Activity. The tested compounds showed diverse but mostly strong antiproliferative effect on the

Table 1. In Vitro Inhibition of Tumor Cell Growth by Compounds 5a−19

	IC_{50} (μM)[a]				
compd	MOLT-4	HCT116	SW620	MCF-7	H460
5a	NT	7 ± 3	NT	7 ± 7	3 ± 0.1
5b	2 ± 0.2	2 ± 0.02	2 ± 0.01	2 ± 0.1	2 ± 0.2
5c	2 ± 0.1	3 ± 1	2 ± 0.1	3 ± 0.4	2 ± 0.3
5d	2 ± 0.4	2 ± 0.02	1 ± 0.2	2 ± 0.1	2 ± 0.2
5e	2 ± 0.5	3 ± 0.03	2 ± 0.1	5 ± 4	2 ± 0.1
6a	2.1 ± 1.4	1.8 ± 0.1	1.2 ± 0.1	1.6 ± 0.01	1 ± 0.2
6b	2 ± 0.9	2.8 ± 0.5	1.3 ± 0.2	2 ± 0.1	1.4 ± 0.1
6c	1.9 ± 0.1	1.7 ± 0.02	1.4 ± 0.1	1.5 ± 0.1	2.6 ± 0.4
7a	1 ± 0.1	1 ± 0.2	1 ± 0.1	2 ± 0.1	2 ± 0.4
7b	1 ± 0.2	0.4 ± 0.03	0.4 ± 0.01	2 ± 0.1	2 ± 0.1
7c	1 ± 0.4	1 ± 0.01	0.4 ± 0.01	2 ± 0.1	2 ± 0.1
7d	2 ± 0.2	2 ± 0.02	2 ± 0.01	3 ± 1	23 ± 4
7e	1 ± 0.7	2 ± 0.7	1 ± 0.5	3 ± 0.2	3 ± 1
9a	0.8 ± 0.4	0.9 ± 0.3	0.7 ± 0.2	1.4 ± 0.1	1.6 ± 0.1
9b	0.8 ± 0.3	1.3 ± 0.1	1.2 ± 0.2	1.5 ± 0.1	1.2 ± 0.1
9c	3 ± 0.4	≥10	≥10	≥10	≥10
10a	8.7 ± 0.8	>10	>10	>10	>10
10b	≥10	>10	>10	>10	>10
11a	0.4 ± 0.03	0.4 ± 0.1	0.2 ± 0.03	1.3 ± 0.2	0.6 ± 0.02
14	1.8 ± 0.2	1.9 ± 0.6	0.9 ± 0.2	1.8 ± 0.2	0.4 ± 0.1
15	3.3 ± 0.8	3.2 ± 0.2	2.1 ± 0.4	2.3 ± 0.1	1.3 ± 0.1
18	4.8 ± 0.3	>10	>10	>10	>10
19	2 ± 0.04	1 ± 0.1	0.3 ± 0.1	2 ± 0.2	1 ± 0.3

[a] IC_{50}: the concentration that causes 50% growth inhibition ± SD.

dx.doi.org/10.1021/jm300505h | *J. Med. Chem.* 2012, 55, 5044−5060

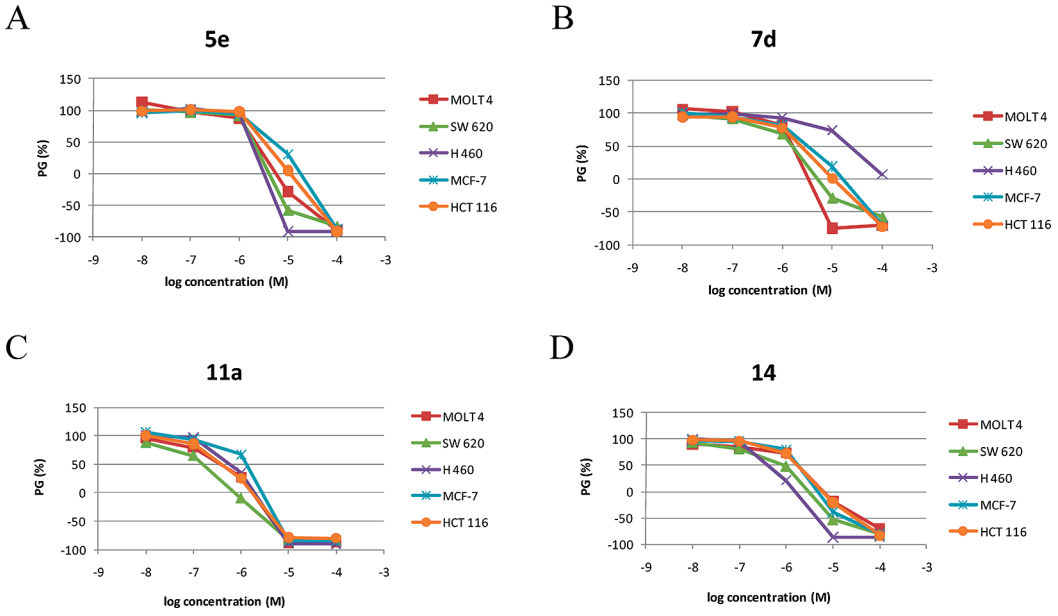

Figure 4. Concentration–response profiles of compounds **5e**, **7d**, **11a**, and **14**. PG = percentage of growth.

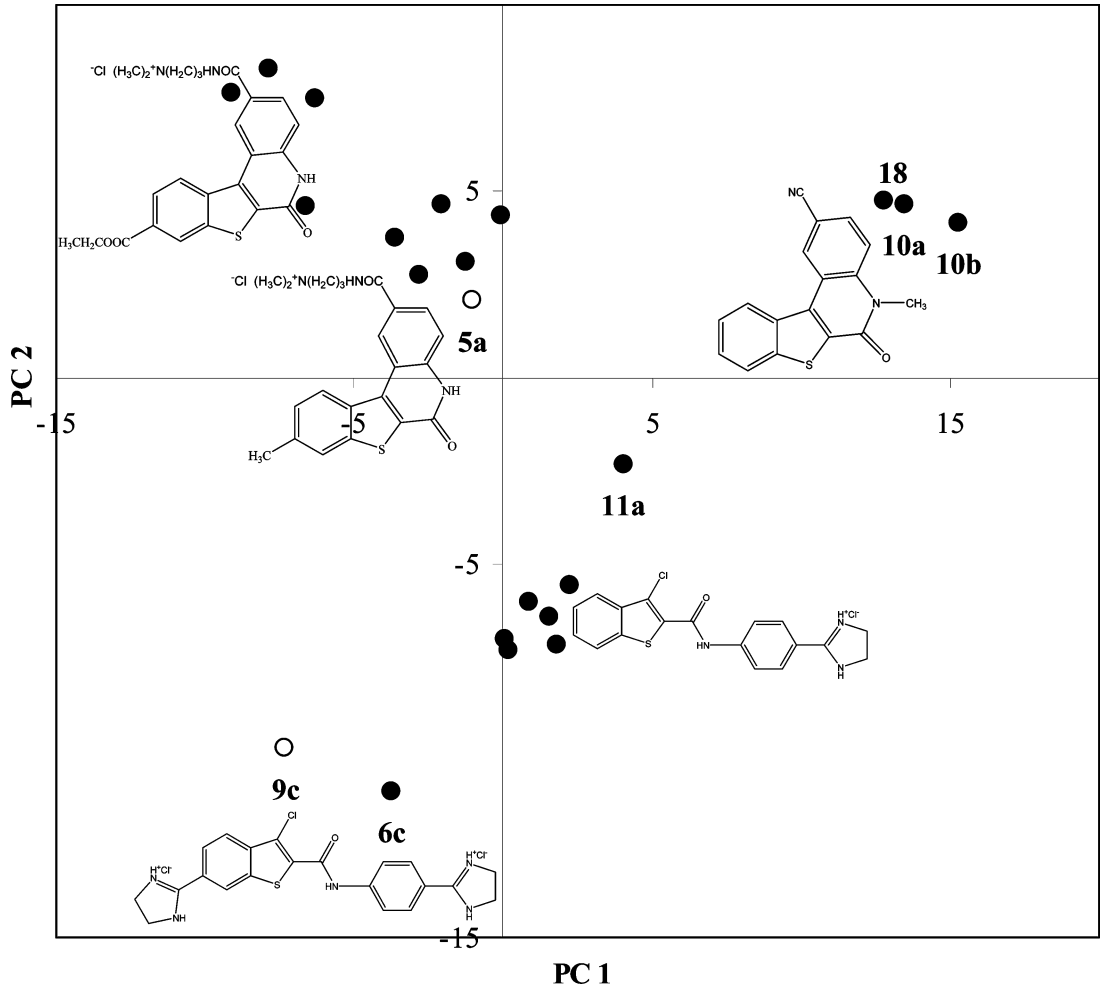

Figure 5. PCA scores plots derived using autoscaling pretreatment.

presented panel of cell lines (Table 1 and Figure 4). All compounds except nitro-substituted carboxanilide **5d**, unsubstituted **7a**, and carbethoxy-substituted **7e** quinolones along with 2-imidazolinyl-substituted carboxianilides **6a–c** and **14** and quinolones **9a** and **9b**, **11a**, and **19** precipitated when diluted with the cell culture medium at the maximal tested

dx.doi.org/10.1021/jm300505h | J. Med. Chem. 2012, 55, 5044–5060

concentration. Because of the lower solubility in aqueous medium of compounds **9c**, **10a**, **10b**, and **15**, the highest tested concentration was 10^{-5} M.

Modest antiproliferative effect was achieved with compounds **5a**, **9c**, **10a**, and **10b**. All other compounds showed very strong and mostly nonselective cytotoxic effect to all tested tumor cell lines. Compounds **5e**, carbethoxy-substituted *N*,*N*-dimethylaminopropylcarbamoylbenzo[*b*]thiophene anilide, and **7d**, nitro-substituted *N*,*N*-dimethylaminopropylcarbamoylbenzo[*b*]thieno[2,3-*c*]quinolin-6-one showed somewhat differential effect on the tumor cell lines (Figure 4A,B). Importantly, the strongest antiproliferative effect (IC_{50} in the submicromolar range) showed the 2-imidazolinyl-substituted derivatives **9a**, **11a**, and **14** (Figure 4C,D).

No significant difference in IC_{50} values was observed between carboxanilide (acyclic) and quinolone (cyclic) derivatives. Similarly, our previously published results also showed similar IC_{50} values after the treatment with acyclic (pyridylbenzo[*b*]-thiophene-2-carboxamides) and cyclic (benzo[*b*]thieno[2,3-*c*]naphthyridin-2-ones) compounds.[9] Still, a minor structural modification (the position of herocyclic nitrogen with respect to amidine substitutent) altered the target specificity and consequently the mode of action.[9] Yet again, the 2-imidazolinyl-substituted derivatives showed the most prominent activity; i.e., the 2-imidazolinyl substituent acts as the best pharmacophoric group in a diverse set of compounds.[9,13,14]

Analysis of the 3D Structure−Activity Relationship. In order to elucidate the structural variables important for the anticancer activity of the analyzed compounds, we performed a detailed chemometric analysis.

Principal Component Analysis (PCA). Principal component analysis (PCA) was performed on the overall data set of 22 compounds using autoscaling pretreatment. The first two principal components explained 61.3% of variance (the first three PCs explained 71.6%).

Distribution of the compounds in the PC space (PC scores) was examined in order to try to find possible grouping of the molecules. From the PCA scores plots (Figure 5) it can be seen that all poorly to moderately active compounds (**10a**, **10b**, **18**) are grouped together. In the space of the first two PCs (Figure 5), they are gathered in the upper-right quadrant. The exception is **9c**, a quinolone with two 2-imidazolinyl substituents, with comparable activity but at the PC plots far from them (Figure 5). However, it is separated from the other compounds as well. The closest compound is carboxanilide **6c** which, similar to **9c**, has two 2-imidazolinyl substituents. Apparently, the structural descriptors of **9c** differ from the other quinolones, and they are mostly determined by the 2-imidazolinyl substituents.

3D-Derived QSAR Models. The 3D-based QSAR models were derived for the compounds analyzed in this work but also for the larger set of compounds including 10 compounds selected from the previous publications[7,9] (Supporting Information Table S2). For this purpose compounds were selected that are structurally similar to the presented ones (i.e., do not significantly expand the space described by the first two principal components shown in Figure 5; see Supporting Information Figure S1) and that, at the same time, cover a wide range of activity. However, previously the antitumor activity tests were performed on different sets of cell lines, with only MCF-7 and SW620 lines common to all studies.

The 3D-derived QSAR models were distinguished according to the variable pretreatment, number of objects, and cell lines (see the methodological part/computational analysis). The models obtained for the antitumor activity of the compounds on the MCF-7 cell line (breast carcinoma) were named **1** (**A**, **B**, **C**, and **D**). Those for the antitumor activity on HCT116 (colon carcinoma) were named **2** (**A** and **B**). Models for the antitumor activity on SW620 (colon carcinoma) were named **3** (**A**, **B**, **C**, and **D**). Models obtained for the antitumor activity on H460 cells (lung carcinoma) were named **4** (**A** and **B**), and models derived for MOLT-4 cell line (T-lymphoblast leukemia) were named **5**. Statistical properties of the models derived using the extended data set are summarized in Table 2. The properties of the models derived using only compounds from the present study are given in Supporting Information Table S3.

Table 2. Statistical Properties of the Four Selected 3D-Derived QSAR Models Derived for the Extended Data Set[a]

model	nO[d]	nLV[e]	R^2	SDEC[f]	Q^2 [g]	SDEP[h]
1C[b]	30	5	0.93	0.15	0.68	0.32
1D[c]	30	6	0.87	0.21	0.60	0.36
3C[b]	30	6	0.94	0.17	0.67	0.39
3D[c]	30	7	0.91	0.21	0.71	0.36

[a] **1** and **3** are models for MCF-7 and SW620 cell lines, respectively. [b] 3D-derived QSAR models obtained for the autoscaled data. [c] 3D-derived QSAR models obtained for the raw data. [d] Number of objects used to built the model. [e] Number of latent variables. [f] SDEC is standard deviation of error of calculation. [g] Q^2 is the cross-validated predictive performance and is given by $Q^2 = 1 - (\sum_{n=1}^{n}(y_{exp(i)} - y_{pred(i)})^2)/\sum_{n=1}^{n}(y_{exp(i)} - \langle y_{exp}\rangle)^2$, where $y_{pred(i)}$ corresponds to the predicted and $y_{exp(i)}$ to the experimentally determined inhibition pIC_{50} for the compound *i*, respectively. [h] SDEP is the standard deviation in cross-validated prediction and is given by SDEP = $[(\sum_{n=1}^{n}(y_{exp(i)} - y_{pred(i)})^2)/n]^{1/2}$.

Models derived for the extended (30 molecules) data set span a large range of biological activities, and although more robust than the above-discussed models, they have good internal and external predictive performances (Table 2). Correlations between measured predicted activities by these models are displayed in Figures 6 and 7.

Compounds **5a** and **9c** turned out to be outliers, and they were omitted from all models. Activity measurements for the compound **5a** are/were very problematic (see Table 1), and the **9c** structural variables significantly differ from those of the other poorly active compounds, as shown by the PC analysis and that might be ascribed to poor solubility of **9c**.

External prediction of the 3D-derived QSAR models was tested using compound **19** as well as compounds **5a** and **9c** (Table 3). The external predictive performances of the models derived using the large data set are better (for compound **19**) or comparable with the external prediction achieved by the models derived considering only compounds from the present study.

Molecular Descriptors with the Highest Impact on the Antitumor Activity. In the 3D-derived QSAR models built with the autoscaled structural variables, the influence of the descriptors to the model can be estimated from their PLS coefficients. Plots with the PLS coefficient for the models **1A**, **2A**, **3A**, **4A**, **1C**, and **3C** (Supporting Information Figures S3 and S4) revealed descriptors related to hydrophilic properties of the compounds, their solubility, and the possibility to make H-bonds as the most important ones. The following descriptors were found to have the highest positive impact on the activity: integy moments (**IW1**−**IW3**) which indicate concentration of

dx.doi.org/10.1021/jm300505h | J. Med. Chem. 2012, 55, 5044−5060

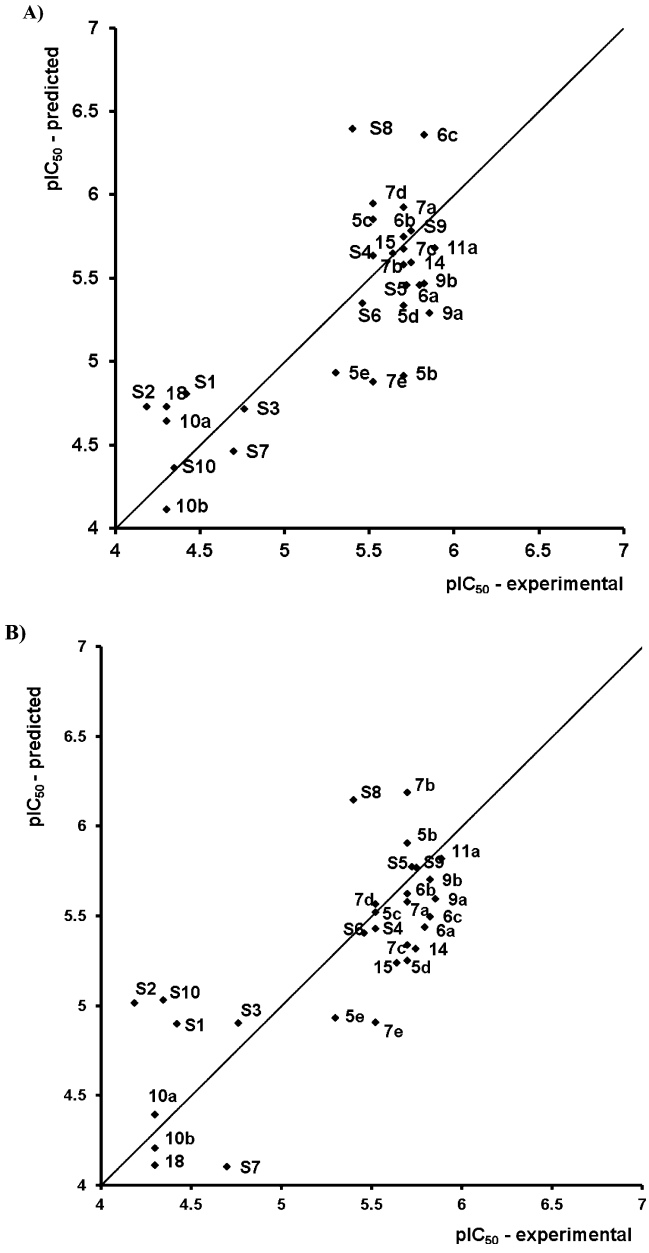

Figure 6. Predicted vs experimental antitumor activity expressed as pIC_{50}, which is the negative logarithmic value of concentration that causes 50% growth inhibition of the MCF-7 tumor cell lines: (A) model **1C**; (B) model **1D**. Some of the compounds are not labeled on the graph for clarity.

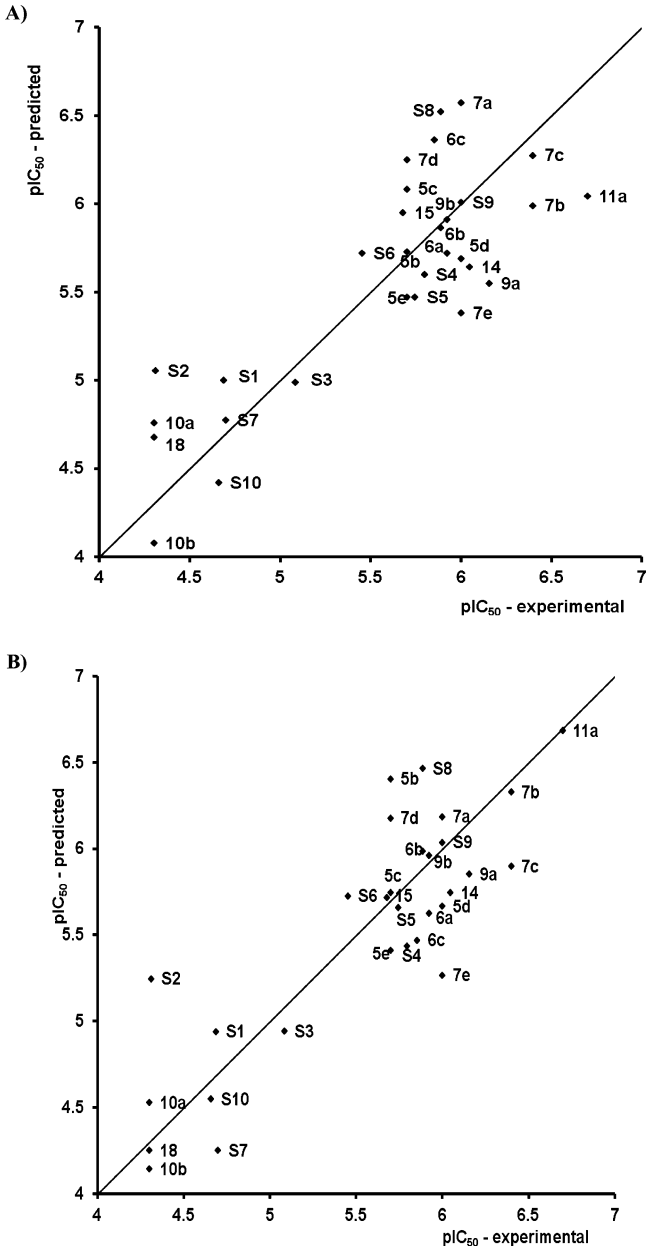

Figure 7. Predicted vs experimental antitumor activity expressed as pIC_{50}, which is the negative logarithmic value of concentration that causes 50% growth inhibition of the SW620 tumor cell lines: (A) model **3C**; (B) model **3D**. The compounds from the previous study are labeled as "**S**".

hydrophilic regions on one part of the molecule, 3D pharmacophoric descriptors related to H-bonding (**DRDRDO**, **DRDRDR**, **DRACDO**, **DRDODO**, **DRDRAC**), and solubility properties (**L2LgS**). Descriptors that were found to have negative correlation with antitumor activity according to the autoscaling 3D-derived QSAR models were lipophilicity (log *P*, especially in the case of the QSAR models derived for the 30-object data set; see **S4**), percentage of un-ionized species at pH range from 4 to 7 (%FU4−%FU7), the ratio of the polar surface area (PSA) to the surface (S) (PSAR), the ratio of the polar surface area (PSA) to the hydrophobic surface area (HSA) (PHSAR), and the capacity factors (CW1−CW3) which represent the ratio of the hydrophilic volume to the total molecular surface.

Molecular Mechanism of Action. Compounds **6a−c**, **9a−c**, and **11a** were selected for further biochemical analysis to investigate their activity regarding DNA binding and topoisomerases targeting of a small series of those compounds as part of their mechanism of action.

DNA Binding Properties. We first focused on the DNA binding ability of this series of molecules using spectrophotometric measurements. For this purpose, the DNA binding propensity was investigated globally through their capacity to increase the melting temperature of double strand DNA during the process of heat denaturation. The induced variations (ΔT_m) were determined for different compound/bp ratios, and the results are presented in Table 4.

dx.doi.org/10.1021/jm300505h | *J. Med. Chem.* 2012, 55, 5044−5060

Table 3. Antitumor Activity of Compounds 19 (Top Rows), 5a (Three Bottom Rows), and 9c against Four Cell Lines Predicted by 3D-Derived QSAR Models

	IC_{50} (μM)[a]			
	HCT116	SW620	MCF-7	H460
experimental	1 ± 0.1	0.3 ± 0.1	2 ± 0.2	1 ± 0.3
predicted by models				
1A, 2A, 3A, 4A[b]	1.15	1.02	2.45	1.26
1B, 2B, 3B, 4B[c]	1.51	0.91	2.69	3.39
1C, 3C[b]		0.38	1.86	
1D, 3D[c]		0.51	2.88	
experimental	7 ± 3	NT	7 ± 7	3 ± 0.1
predicted by models				
1A, 2A, 3A, 4A[b]	1.82	1.18	1.03	1.21
1B, 2B, 3B, 4B[c]	2.88	2.10	1.41	2.14
1C, 3C[b]		0.72	1.78	
1D, 3D[c]		1.82	3.16	
experimental	≥10	≥10	≥10	≥10
predicted by models				
1A, 2A, 3A, 4A)[b]	0.55	0.35	0.28	1.72
1B, 2B, 3B, 4B[c]	1.96	1.68	1.18	1.28
1C, 3C[b]		0.78	1.45	
1D, 3D[c]		2.04	3.16	

[a]The concentration that causes 50% growth inhibition. [b]3D QSAR models obtained for the autoscaled data. [c]3D QSAR models obtained for the raw data.

From this series, the carboxanilide **6c** and quinolone **9c** derivatives bearing two 2-imidazolinyl substituents were identified as the most potent compound to stabilize the DNA helix with ΔT_m larger than 20 °C at R = 0.25. Their corresponding monoimidazolinyl substituted analogues (**6a,b** and **9a,b**) as well as the N-methylated derivative **11a** were less potent in the DNA helix stabilization. Interestingly, the quinolones (**9a,b** and **11a**) were more potent than the carboxanilides (**6a,b**) with ΔT_m between 10 and 20 °C at R = 0.25 for the former and below 10 °C for the later derivatives. Similarly, UV/visible spectrometry identified the lowest hypochromic effects using the monoimidazolinyl substituted carboxanilides **6a,b** (Figure 8). An isosbestic point was obtained using compound **6c** at CT-DNA up to 100 μM (exemplified panel, as indicated by the arrows), suggesting a single mode of binding in this concentration range. For all other compounds, no isosbestic points were observed when increasing the DNA concentration, suggesting that they do not present a unique mode of binding to the DNA.

To get an insight into the mode of binding (groove binding versus intercalation) of these compounds to the DNA, we tested them for both circular dichroism and topoisomerase I induced relaxation of supercoiled plasmid DNA (Figure 9). Circular dichroism spectra were collected in BPE buffer supplemented or not with increasing concentration of NaCl. Incubation of **6c** in the CT-DNA solution resulted in a large, positively induced CD (ICD) peak with its maximum at ∼325 nm (Figure 9C, lanes light blue, pink, and purple) suggesting the groove binding of the biimidazolinyl-substituted carboxanilide **6c**. This strong positive ICD is also present upon incubation in buffer containing 10 mM (Figure 9C, orange line) or 100 mM NaCl (Figure 9D), suggesting strong binding in the groove, even at high salt concentrations. Compounds **6a** and **6b** induced a weak bisignate ICD around 340 and 355−390 nm, respectively, suggesting intermolecular stacking of these molecules in the presence of CT-DNA at the highest concentration. Once again, this modified CD is also observed upon addition of 10 (orange lines) and 100 mM (red lines) NaCl.

The 3D-derived QSAR analysis revealed that integy moments, which indicate concentration of hydrophilic regions on one part of the molecule, and 3D pharmacophoric descriptors related to the hydrogen bond formation potency are positively correlated with the biological activity. These descriptors, combined with the large planar platform, are desirable for DNA binders, and in agreement with the measured DNA binding properties, they are accentuated in compounds **11a** and **9c**. Activity of **9c** was significantly overestimated by the 3D-derived QSAR models where it was considered as an outlier. The experiments on DNA binding properties showed that this compound is indeed a strong DNA binder with minor groove and intercalative profiles. However, this DNA binding propensity does not lead to a particularly strong antitumor activity relative to the other compounds. A possible reason might be low solubility.

The DNA intercalation potency of this series was evaluated using topoisomerase I induced DNA relaxation assays (Figure 10). Incubating a supercoiled plasmid DNA with an

Table 4. Variations of the DNA Melting Temperature upon Binding of the Compounds ($\Delta T_m = T_{m[Drug+DNA]} - T_{m[DNAalone]}$) Determined at Different Drug/bp Ratios (R)[a]

	ΔTm (°C)				
Compound	R=0.01	R=0.025	R=0.1	R=0.25	R=0.5
6a	*nd*	*nd*	*nd*	5	6.8
6b	*nd*	*nd*	*nd*	3	3.8
6c	1	2	7.9	23.9	28.4
9a	0	0.9	4.9	18	*na*
9b	*nd*	*nd*	*nd*	11	14.6
9c	0	0	15.7	22.4	*na*
11a	*nd*	*nd*	*nd*	10.7	15.6

[a]nd: not determined. na: could not be analyzed. Light gray: strong binding when 10 °C < ΔT_m < 20°C. Dark gray: very strong binding with ΔT_m > 20°C.

dx.doi.org/10.1021/jm300505h | J. Med. Chem. 2012, 55, 5044−5060

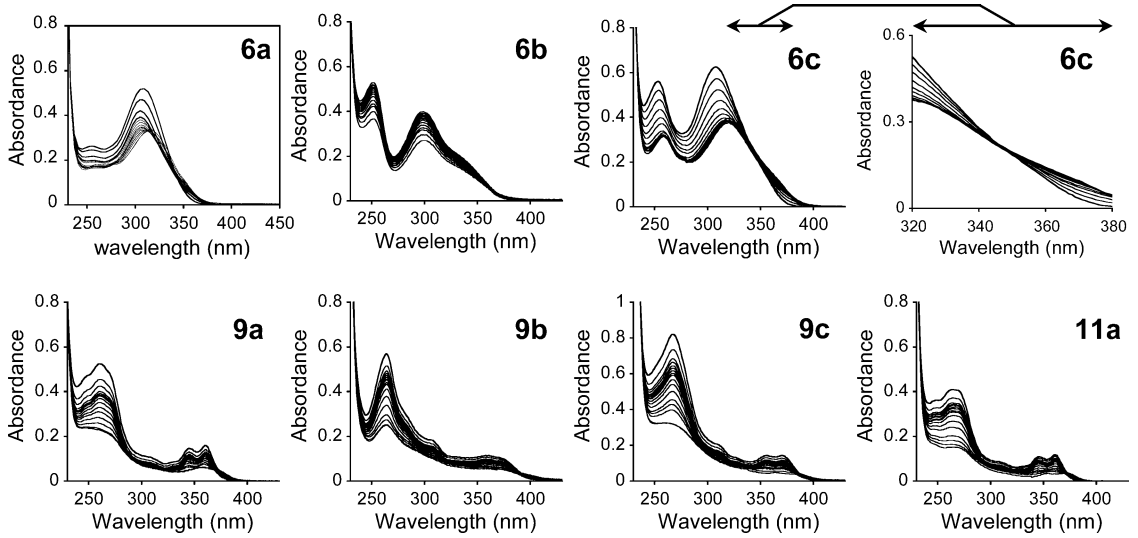

Figure 8. UV/vis spectra of drug–DNA interaction. An amount of 20 μM each compound was incubated alone (top lines) or with step by step increasing concentrations of CT-DNA from 10 to 200 μM (**6a** and **6c**) or from 0.1 to 40 μM (**6b**, **9a–c**, and **11a**). Each spectrum is recorded from 230 to 430 nm relative to a cuvette containing the same amount of CT-DNA, with the upper right panel being an example of the previous panel (arrows) focusing on the isosbetic point indicated with the presence of increasing concentrations of **6c** (up to 100 μM).

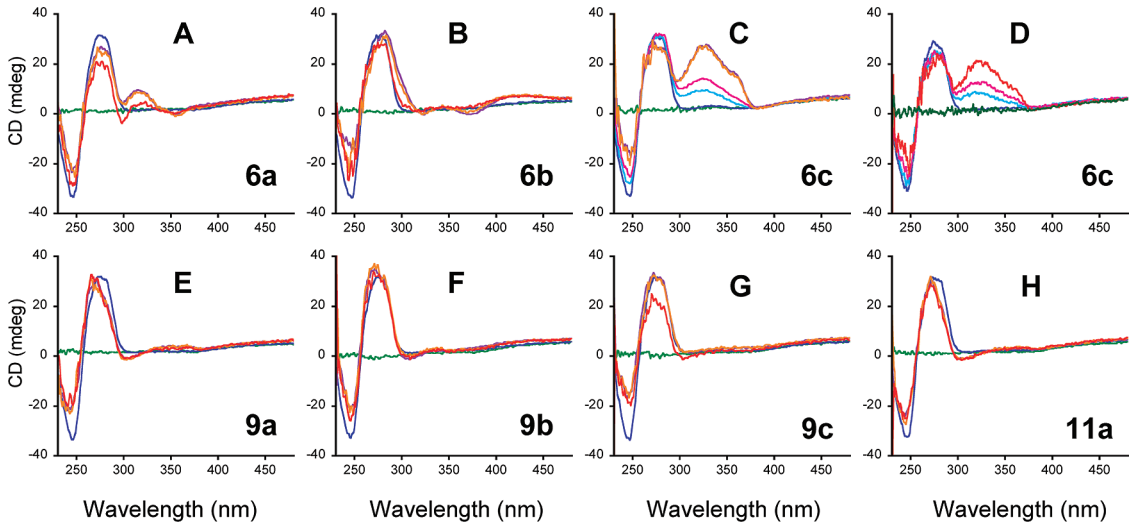

Figure 9. Circular dichroism spectra. CT-DNA (200 μM, blue lines) was incubated with 50 μM **6a**,**b**, **9a–c**, or **11a** in BPE buffer (purple lines) supplemented with 10 mM (orange lines) or 100 mM (red lines) NaCl. For compound **6c**, CT-DNA was incubated in BPE supplemented with 100 mM NaCl (D) or 10 mM NaCl (orange line in C) or in BPE (all other lanes in C) in the presence of 10 μM (light blue lines), 20 μM (pink lines), or 50 μM (purple, orange or red lines for BPE, BPE + 10 mM NaCl, or BPE + 100 mM NaCl buffers, respectively). The absence of intrinsic CD of the molecules is visualized as green lines.

intercalating drug led first to a decrease of the number of supercoils in topoisomers, up to a fully relaxed (circular) DNA followed by switching back to topoisomers with a progressive increase of the number of supercoils in the positive orientation, opposite to the negative supercoils naturally occurring in plasmids produced in bacteria.[15] The experiment showed that the condensed structures **9a–c** and **11a** are potent DNA intercalating drugs. The intermediate stage corresponding to the fully relaxed form ("Rel", Figure 10) is reached using weak concentrations of these compounds (0.5–2 μM), close to that obtained using ethidium bromide (0.25 μM) in similar experiments.[15] In contrast, molecules with the carboxanilide core **6a–c** characterized by higher flexibility (and a smaller coplanar platform) showed lower DNA intercalating properties, as evidenced from fully relaxed DNA that is reached using ~10 μM (**6a**, **6c**) or ~50 μM (**6b**).

The potential sequence specificity of the compounds was first tested using DNase I footprinting. Sequence-selective binding was observed for binding of the compounds to the DNA groove (minor), regarding its circular dichroism spectra, **6c**. Densitometric analysis revealed weak sequence selectivity of **6c** for the AT-rich sites (the gray boxed regions in the graph at the bottom of Figure 11). The other tested compounds have not shown any sequence selectivity but global inhibition of DNase I cleavage, typical for DNA intercalators. Therefore, DNase I footprinting is in agreement with previous results.

To comfirm the potent binding of **6c** to AT-rich sequences, we performed both melting temperature and spectroscopic (UV/visible and circular dichroism) studies on poly(dAdT)$_2$

dx.doi.org/10.1021/jm300505h | J. Med. Chem. 2012, 55, 5044–5060

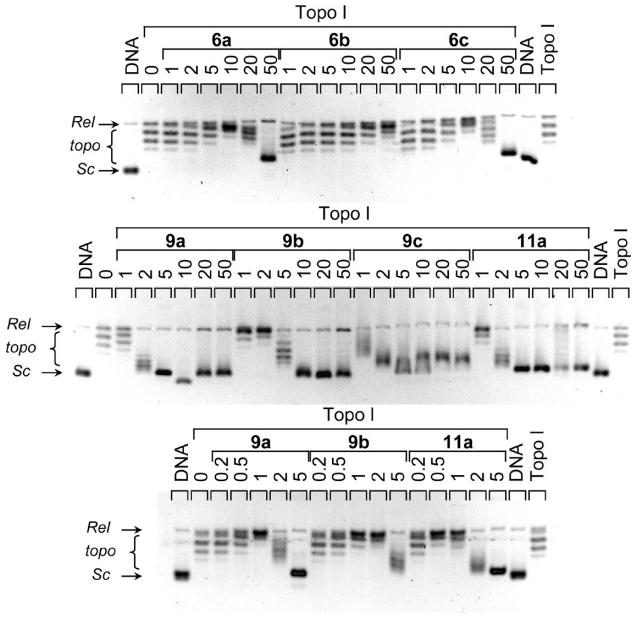

Figure 10. Topoisomerase I induced DNA relaxation. Various concentrations of compounds (as indicated in micromolar at the top of each lane) were incubated with supercoiled (Sc) pUC19 plasmid prior to treatment with topoisomerase I enzyme (Topo I) to reveal relaxed plasmid (Rel) and various topoisomers (topo). DNA, untreated supercoiled plasmid DNA.

(Figure 12). The high ΔT_m values obtained at low drug/DNA ratios are evidence of the strong **6c** binding to poly(dAdT)$_2$. CD spectra with a maximum peak shifting from ~330 nm (maximum at 20 μM, green line) to ~365 nm (max at 100 μM, red line) followed by rapid decrease from 100 to 200 μM indicated binding of **6c** into the groove of poly(dAdT)$_2$ DNA.

Topoisomerase I or II Inhibition Properties. Functional evaluation of topoisomerase I inhibition by compounds **6a−c**, **9a−c**, and **11a** was first evaluated in terms of poisoning activity on denaturing polyacrylamide gels using CPT as a reference drug. It was found (Supporting Information Figure S5A) that none of the tested compounds poisoned topoisomerase I (no cleaved band was visualized). Further, we found that their potency to suppress the topoisomerase I activity is related with their binding to the DNA (Supporting Information Figure S5B). The most potent compounds were **6c** and **9b** with full inhibition obtained at 10 μM. Such suppressor activity is in correlation with their strong DNA binding propensities, as indicated from DNA melting temperature studies (Table 4).

Finally we evaluated compound activity as topoisomerase II inhibitors. Etoposide was used as a reference drug. Its ability to block the ligation step is classically revealed by the appearance of a new DNA band corresponding to linearized plasmid DNA ("Lin"). We found (Figure 13) that compounds **6a−c** and **9a−c**, but not **11a**, efficiently inhibited topoisomerase II enzyme. Quantification relative to the same concentration (50 μM) of etoposide (lanes "Etop") showed that **6a** was as potent as etoposide on Topo II.

We found compounds **6c**, **9c**, and **11a** as the most outstanding ones, the first two as the most potent DNA binder and the third as the only one that did not inhibit topoisomerase II activity. The results obtained for DNA binding propensities and topoisomerases I and II inhibition prompted us to compare descriptors for **6c**, **9c**, and **11a** (Figure 14). Apparently, **6c** and **9c** are more hydrophilic than the third one (descriptors W1−W5), and their potency to take part in hydrogen bond formation as proton donors is 2 times higher than the potency of **11a** (descriptor WO1). On the other hand, values of %FU descriptors, which were found to negatively correlate with the biological activity by QSAR analysis, point to the possibility of **11a** to become neutral at high pH values. Neutrality could not be considered as a desirable characteristic for DNA binders but can facilitate binding to the hydrophobic pocket of a protein, suggesting that this compound could exert its cytotoxic effect through another mechanism of action than **6c** and **9c**.

Cell Cycle Perturbations. We selected compounds **6a**, **6c**, **9a**, and **11a** as the most active and interesting representatives of carboxanilides and quinolones that, as discussed earlier, showed interesting and different DNA binding features. All compounds were tested for cell cycle perturbation on the HCT 116 cell line for 24 and 48 h using flow cytometry. Concentration that was used was ~IC$_{50}$ (1 μM) or slightly higher than IC$_{50}$ (5 μM) of all compounds (Figure 15). All of the compounds induced time- and concentration-dependent effects on the cell cycle. Interestingly, only **6a** at the higher concentration induced statistically significant accumulation of cells in the G1 phase of the cell cycle, pointing to cellular target(s) other than DNA for this compound, which is in agreement with its low DNA-binding activity but not with the Topo II inhibitory activity. All other compounds induced accumulation of cells in the G2/M phases, accompanied by the reduction of cells in the S phase, correlating with the DNA damage mechanism. Namely, the accumulation of cells in G2/M phases (a G2/M phase arrest) points to a damage in the cell, which occurs during the S phase (DNA replication) or before mitosis (aberrant mitotic spindle formation). Thus, it is usually triggered by agents that induce DNA damage or mitotic spindle damage. As expected, **6c** displayed a rather moderate effect on the cell cycle perturbations, with an increase in the G2/M, after the treatment with the higher concentration and after a prolonged period of treatment. The quinolones **9a** and **11a** induced a strong G2/M arrest, along with a drastic S phase reduction, whereas compound **9a**, which also induced apoptosis (indicated by the subG1 percentage), is more effective. This was expected from their high antiproliferative activity (submicromolar IC$_{50}$) and strong intercalation into double stranded DNA. However, since **11a** was shown to have different relative physicochemical characteristics from the other compounds used to build the QSAR model and since it seems that its high cytotoxicity is achieved by different mode of action, it could also be possible that its activity may interfere with the cellular tubulin level which, leading to mitotic spindle damage, can also induce G2/M arrest.

■ CONCLUSION

A series of carboxanilides (**5a−e**, **6a−c**, and **14**) and quinolones (**7a−e**, **9a−c**, **10a**, **10b**, **11a**, **11b**, **17**, and **19**) were prepared and tested for the antiproliferative activity on various tumor cell lines. In general, all compounds except cyano-substituted quinolones showed very prominent activity, whereby 2-imidazolinyl-substituted ones were among the most active. Further, some of them, **6a−c**, **9a−c**, and **11a**, were evaluated for DNA binding propensities and topoisomerases I and II inhibition in order to learn about their mechanism of action.

The 3D-derived QSAR analysis was performed for the data set consisting of compounds from present and previous studies. The highly predictive 3D-derived QSAR models were derived, and molecular properties that have the highest impact on

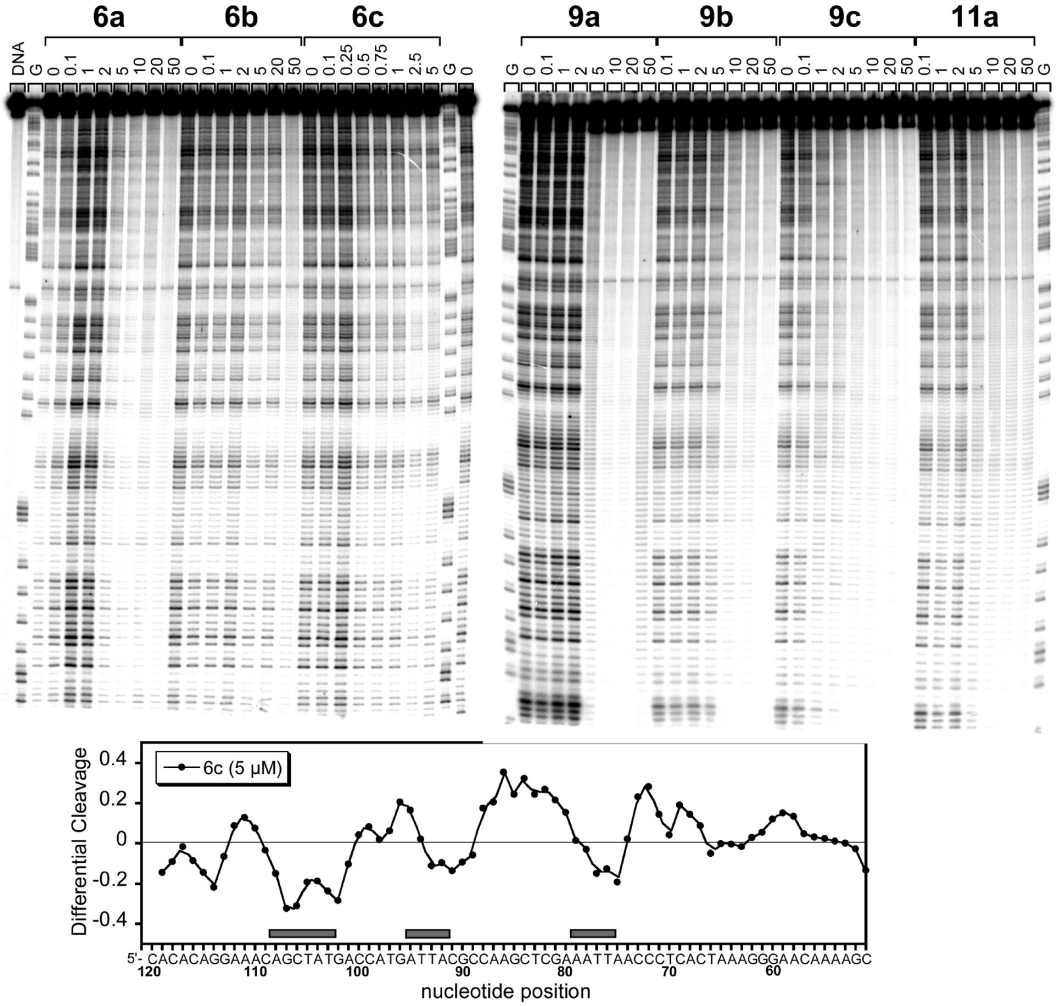

Figure 11. DNase I footprinting assays. Denaturing polyacrylamide gel in the presence of the various tested compounds (top) and the densitometric analysis (bottom) of the sequence-selective binding of **6c** on the 3′-end radiolabeled 265 bp DNA fragment. Gray boxes exemplify compound localization on the DNA helix relative to its base pair composition. DNA, DNase-I untreated 265 bp fragment used as quality control. The G-track was used to localize guanines in the DNA fragment and to deduce the migration position of each base within the known sequence.

antitumor activity of carboxanilides and quinolones were identified. The results of 3D-derived QSAR analysis nicely agree with the results obtained for DNA binding propensities and topoisomerases I and II inhibition measurements. The most potent DNA binders, **6c** and **9c**, are grouped together in the PCA score plot (Figure 5). In the same plot compound **11a**, for which no effect on topoisomerase II inhibition was found, is close to the origin and isolated from the other compounds. However, while **6c** binds to DNA as a groove binder, **9c** binds to DNA as an intercalator. By five 3D-derived QSAR models (**1A**, **1B**, **1C**, **4A**, **4B**) **6c** was predicted to be the most active compound in the series. Among the compounds in the training set, the activities of compounds **6c** and **7a** were, on average, the most overestimated. Compound **11a**, for which no effect on topoisomerase II inhibition was found, is on the PCA score plot close to the origin and isolated from the other compounds, indicating that its mode of action might differ from those of the other active compounds. Its activity was much better predicted with the models derived for the 30-objects data set than with the models considering only compounds from the present study, suggesting robustness of the previous. The cell cycle perturbation experiments showed that **6c** displayed rather a moderate effect on the cell cycle perturbations while the quinolones **9a** and **11a** induced a strong G2/M arrest along with a drastic S phase reduction whereas compound **9a** which also induced apoptosis was more effective. Since **11a** was shown to have different relative physicochemical characteristics from the other compounds used to build the QSAR model, it seems that its high cytotoxicity is achieved by a different mode of action. So it could be possible that its activity may interfere with the cellular tubulin level which, leading to mitotic spindle damage, can also induce G2/M arrest. From the obtained analysis it is clear that there is no unique mode of action of the active compounds analyzed in the present study to achieve their activity. Taken together, the results indicate the most potent directions of development of new anticancer compounds (from the same series), namely, increasing concentration of hydrophilic regions and their clustering at a certain region of the molecular surface, improving H-bonding efficiency, and increasing solubility. Specifically, the presence of 2-imidazolinyl at the fourth position from the amido group (peptide bond) boosts biological activity of thieno compounds.

EXPERIMENTAL SECTION

Chemistry. Melting points were determined on a Koffler hot stage microscope and are uncorrected. IR spectra were recorded on FTIR-

dx.doi.org/10.1021/jm300505h | J. Med. Chem. 2012, 55, 5044−5060

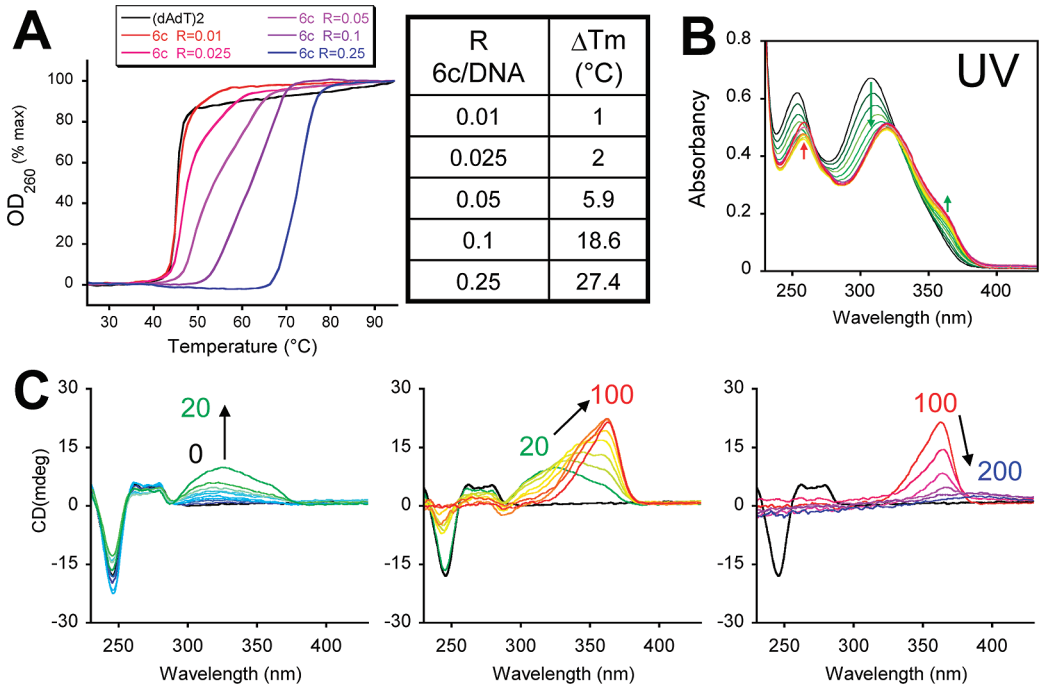

R 6c/DNA	ΔTm (°C)
0.01	1
0.025	2
0.05	5.9
0.1	18.6
0.25	27.4

Figure 12. Sequence-selective binding of **6c** to AT-rich DNA. (A) Variation of the absorbency at 260 nm during the heating process of samples containing poly(dAdT)$_2$ alone (black) or incubated with increasing drug/DNA ratios of **6c**. The ΔT_m values derived from the graph are presented in the table. (B) UV/visible spectrophotometry of **6c** (20 μM) alone (black line) or incubated with increasing concentrations of poly(dAdT)$_2$ from 10 to 200 μM. Major changes are observed below 100 μM (red line) as exemplified by green arrows. Minor spectral modifications appearing between 100 and 200 μM are localized using green arrows. (C) CD spectra of poly(dAdT)$_2$ alone (black lines) or incubated with increasing concentrations of **6c** from 1 to 20 μM (green lines), from 20 to 100 μM (red lines), and from 100 to 200 μM (blue lines).

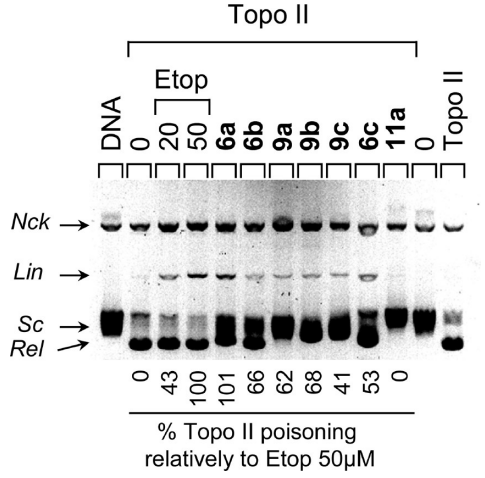

Figure 13. Topoisomerase II poisoning effect. The various tested compounds (50 μM) were incubated with 350 ng of pUC19 supercoiled plasmid DNA prior to addition of Topo II as described.[16] After migration, the gel was quantified for the percentage of topoisomerase II poisoning effect normalized to the reference drug etoposide used at the same concentration.

ATR, Nicolet Magna 760, Perkin-Elmer 297, and Perkin-Elmer Spectrum 1 spectrophotometers, with KBr disks. ^{1}H and ^{13}C NMR spectra were recorded on Varian Gemini 300, Bruker Avance DPX 300, and Bruker Avance DRX 500 spectrometers equipped with a 5 mm broadband probe or on a 14.1 T Varian 600 system (Varian, Palo Alto, CA) equipped with a 3 mm broadband probe using TMS as an internal standard in DMSO-d_6. Mass spectra were recorded with an Agilent 1100 series LC/MSD Trap SL spectrometer using electrospray ionization (ESI). Elemental analyses for carbon, hydrogen, and nitrogen were performed on a Perkin-Elmer 2400 elemental analyzer and a Perkin-Elmer series II CHNS analyzer 2400. Where analyses are indicated only as symbols of elements, analytical results obtained are within 0.4% of the theoretical value. All compounds were routinely checked by TLC with Merck silica gel 60F-254 glass plates. In preparative photochemical experiments the irradiation was performed at room temperature with a water-cooled immersion well with an "Origin Hanau" 400 W high pressure mercury arc lamp using Pyrex glass as a cutoff filter of wavelengths below 280 nm. All compounds were routinely checked by TLC with Merck silica gel 60F-254 glass plates.

General Method for the Synthesis of 2-Imidazolinyl Substituted 3-Chlorobenzo[*b*]thiophene-2-carboxamide Hydrochlorides (6a–c). A stirred suspension of the corresponding carboxamide in absolute ethanol or 2-methoxyethanol was cooled in an ice–salt bath and was saturated with HCl gas. The reaction mixture was maintained at room temperature until the nitrile band disappeared (monitored by IR analysis at 2200 cm^{-1}) and than diluted with diethyl ether. The crude imidate was filtered off and was immediately suspended in absolute ethanol. Ethylenediamine was added, and the mixture was stirred at reflux for 24 h. The crude product was then filtered off, washed with diethyl ether to give a powder which was suspended in absolute ethanol and saturated with HCl (g). The reaction mixture was stirred at room temperature for 24 h. The products were filtered off.

***N*-[4′-(*N*′-2-Imidazolinyl)phenyl]-3-chlorobenzo[*b*]-thiophene-2-carboxamide Hydrochloride (6a).** Compound **6a** is prepared using above-described method. A solution of compound **2f**[7] (0.60 g, 1.92 mmol) in absolute ethanol (25 mL) was saturated with HCl gas and stirred until the nitrile band disappeared. The crude imidate was filtered off and was immediately suspended in absolute ethanol (25 mL). Ethylenediamine (0.45 mL, 6.75 mmol) was added. The mixture was stirred at reflux for 24 h, and 0.50 g (61%) of white solid was obtained, mp >270 °C. IR ν/cm^{-1}: 3078, 2968, 1647, 1605, 1529. ^{1}H NMR (DMSO-d_6) (δ ppm): 11.14 (s, 1H, NH$_{amide}$), 10.84 (s, 2H, NH$_{amidine}$), 8.20–8.18 (m, 1H, H$_{arom}$), 8.16 (d, 2H, J = 8.9 Hz, H$_{arom}$), 7.99 (d, 2H, J = 8.9 Hz, H$_{arom}$), 7,97–7,96 (m, 1H, H$_{arom}$),

dx.doi.org/10.1021/jm300505h | J. Med. Chem. 2012, 55, 5044–5060

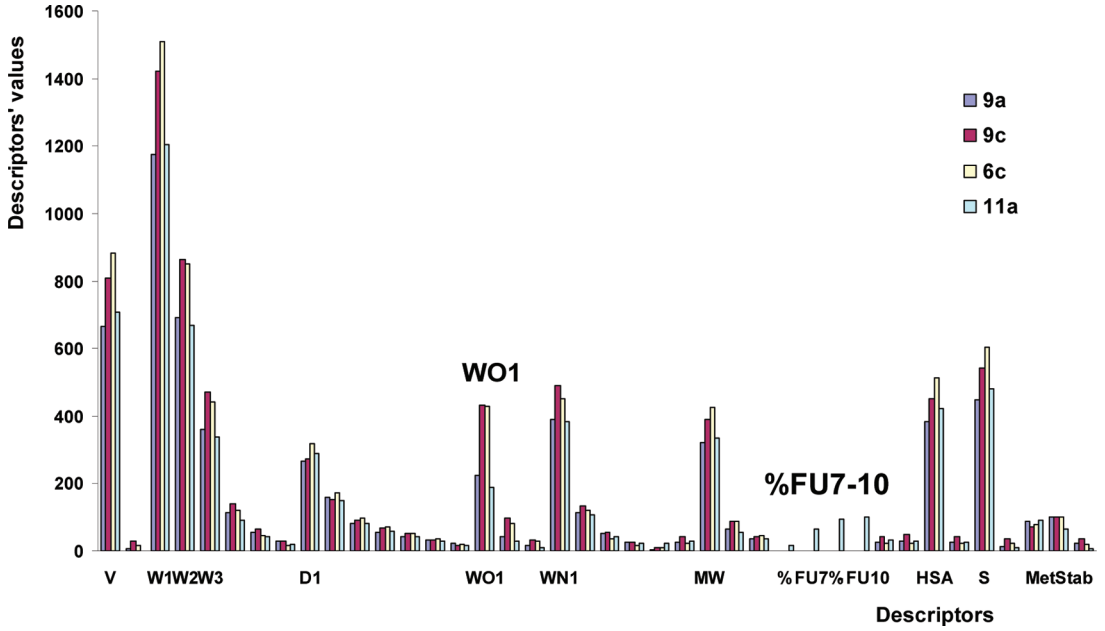

Figure 14. Volsurf+ descriptors for compounds **6c** (blue), **9c** (red), and **11a** (green). Only descriptors with absolute values above 15 are shown, and only the most pronounced ones are labeled. Labels of the descriptors with values notably differing among **6c** (blue), **9c** (red), and **11a** (green) are given above the axis. List and description of all 128 Volsurf+ descriptors are given in the VolSurf+ manual.[17,18]

7.66−7.64 (m, 2H, H_{arom}), 4.00 (s, 4H, $CH_{2imidazolyl}$). ^{13}C NMR (DMSO-d_6) (δ ppm): 164.0 (s), 159.7 (s), 143.6 (s), 136.8 (s), 135.6 (s), 131.3 (s), 129.9 (d, 2C), 127.8 (d), 126.2 (d), 123.6 (d), 122.6 (d), 120.5 (s), 119.7 (d, 2C), 117.3 (s), 44.2 (t, 2C).

6-(*N*″-2-Imidazolinyl)-*N*-phenyl-3-chlorobenzo[*b*]thiophene-2-carboxamide Hydrochloride (6b). A mixture of compound **2g**[7] (0.50 g, 1.60 mmol) in dry ethanol (25 mL) was saturated with HCl gas and stirred until the nitrile band disappeared. The crude imidate was filtered off and was immediately suspended in absolute ethanol (25 mL). Ethylenediamine (0.35 mL, 5.25 mmol) was added. The mixture was stirred at reflux for 24 h, and 0.24 g (35%) of white solid was obtained, mp >270 °C. IR ν/cm^{-1}: 3050, 2937, 2870, 1644, 1613, 1520. ^1H NMR (DMSO-d_6) (δ ppm): 10.83 (s, 2H, $NH_{amidine}$), 10.75 (s, 1H, NH_{amide}), 8.83 (s, 1H, H_{arom}), 8.22 (d, 1H, J = 8.5 Hz, H_{arom}), 8.12 (d, 1H, J = 8.5 Hz, H_{arom}), 7,73 (d, 2H, J = 7.8 Hz, H_{arom}), 7.41 (t, 2H, J = 7.4 Hz, H_{arom}), 7.19 (t, 1H, J = 7.4 Hz, H_{arom}), 4.07 (s, 4H, $CH_{2imidazolyl}$). ^{13}C NMR (DMSO-d_6) (δ ppm): 164.7 (s), 158.3 (s), 139.4 (s), 138.0 (s), 136.8 (s), 136.4 (s), 128.9 (d, 3C), 125.4 (d), 124.9 (d), 124.7 (d), 123.4 (d), 120.9 (s), 120.3 (s), 119.6 (s), 44.6 (t, 2C).

6-(*N*″-2-Imidazolinyl)-*N*-[4′-(*N*′-2-imidazolinyl)phenyl]-3-chlorobenzo[*b*]thiophene-2-carboxamide Dihydrocloride (6c). A mixture of compound **2h**[7] (0.35 g, 1.04 mmol) in dry 2-methoxyethanol (40 mL) was saturated with HCl gas and stirred until the nitrile band disappeared. The crude imidate was filtered off and was immediately suspended in absolute ethanol (30 mL). Ethylenediamine (0.42 mL, 6.22 mmol) was added. The mixture was stirred at reflux for 24 h, and 0.24 g (47%) of white solid was obtained, mp >285 °C. IR ν/cm^{-1}: 3050, 2911, 2751, 2680, 1659, 1608, 1510. ^1H NMR (DMSO-d_6) (δ ppm): 11.33 (s, 1H, NH_{amide}), 10.97 (s, 2H, $NH_{amidine}$), 10.69 (s, 2H, $NH_{amidine}$), 8.92 (s, 1H, H_{arom}), 8.24 (d, 1H, J = 8.5 Hz, H_{arom}), 8.17 (dd, 1H, J_1 = 8.6 Hz, J_2 = 1.3 Hz, H_{arom}), 8.09 (d, 2H, J = 8.9 Hz, H_{arom}), 7.99 (d, 2H, J = 8.9 Hz, H_{arom}), 4.06 (s, 4H, $CH_{2imidazolyl}$), 4.00 (s, 4H, $CH_{2imidazolyl}$). ^{13}C NMR (DMSO-d_6) (δ ppm): 165.0 (s), 164.5 (s), 159.6 (s), 143.9 (s), 139.7 (s), 137.0 (s), 136.3 (s), 130.4 (d, 2C), 126.0 (d), 125.5 (d), 124.0 (d), 121.6 (s), 120.4 (d, 2C), 118.0 (s), 45.0 (t, 2C), 44.7 (t, 2C).

2-(2-Imidazolinyl)-6-oxo-5,6-dihydro[1]benzothieno[2,3-*c*]-quinolin-6-one Hydrochloride (9a). *Method A.* For the synthesis of **9a** was applied the method described for the compounds **6a−c**. A stirred suspension of **8a** (0.30 g, 1.09 mmol) in absolute ethanol (20 mL) was saturated with HCl gas and stirred until the nitrile band disappeared. The crude imidate was filtered off and was immediately suspended in absolute ethanol (15 mL). Ethylenediamine (0.24 mL, 3.66 mmol) was added, and the mixture was stirred at reflux for 24 h. The crude product was then filtered off, washed with diethyl ether to give a powder which was suspended in absolute ethanol and saturated with HCl (g). The reaction mixture was stirred at room temperature for 24 h, and 0.30 g (78%) of yellow powder was obtained, mp >285 °C.

Method B. A solution of acyclic imidazolinyl-substituted 3-chlorobenzo[*b*]thiophene-2-carboxamide **6a** (0.10 g, 0.23 mmol) in water (35 mL) was irradiated for 2 h at room temperature. The reaction mixture was concentrated under the reduced pressure and filtered off, and 0.08 g (96%) of yellow solid was obtained, mp >285 °C. IR ν/cm^{-1}: 3061, 2957, 1664, 1597. ^1H NMR (DMSO-d_6) (δ ppm): 12.72 (s, 1H, $NH_{quinolone}$), 10.93 (s, 2H, $NH_{amidine.}$), 9.13 (t, 1H, J_1 = 4.9 Hz, J_2 = 3.7 Hz, H_{arom}), 9.02 (s, 1H, H_{arom}), 8.28 (t, 1H, J_1 = 3.9 Hz, J_2 = 5.1 Hz, H_{arom}), 8.14 (d, 1H, J = 8.6 Hz, H_{arom}), 7.70 (t, 3H, J_1 = 5.7 Hz, J_2 = 2.7 Hz, H_{arom}), 4.07 (s, 4H, $CH_{2imidazolyl}$). ^{13}C NMR (DMSO-d_6) (δ ppm): 164.3 (s), 158.1 (s), 141.9 (s), 141.4 (s), 135.3 (s), 135.0 (s), 133.8 (s), 128.5 (d), 128.0 (d), 126.9 (d), 126.2 (d), 124.3 (d), 124.2 (d), 117.5 (d), 117.3 (s), 116.0 (s), 44.7 (t, 2C).

General Method for the Synthesis of 2- and 9-Substituted 6-Oxo-5,6-dihydro[1]benzothieno[2,3-*c*]quinolin-6-ones (9b, c). A solution of 3-chlorobenzo[*b*]thiophene-2-carboxamide derivatives (**6b,c**) in methanol or water was irradiated at room temperature with a 400 W high-pressure mercury lamp for 1.5 and 2 h. The solution was concentrated, and the obtained solid was filtered off.

9-(2-Imidazolinyl)-6-oxo-5,6-dihydro[1]benzothieno[2,3-*c*]-quinolin-6-one Hydrochloride (9b). A solution of **6b** (0.10 g, 0.26 mmol) in methanol (80 mL) was irradiated for 2 h, and 0.08 g (88%) of yellow solid was obtained, mp >285 °C. IR ν/cm^{-1}: 3132, 2988, 1644, 1618. ^1H NMR (DMSO-d_6) (δ ppm): 12.46 (s, 1H, $NH_{quinolone}$), 10.89 (s, 2H, $NH_{amidine.}$), 9.20 (d, 1H, J = 8.8 Hz, H_{arom}), 8.92 (s, 1H, H_{arom}), 8.84 (d, 1H, J = 8.0 Hz, H_{arom}), 8.21−8.17 (m, 1H, H_{arom}), 7.67−7.59 (m, 2H, H_{arom}), 7.48−7.43 (m, 1H, H_{arom}), 4.09 (s, 4H, $CH_{2imidazolyl}$). ^{13}C NMR (DMSO-d_6) (δ ppm): 164.8 (s), 157.9 (s), 141.4 (s), 139.8 (s), 138.2 (s), 135.9 (s), 129.8 (d), 127.0 (d), 125.5 (d, 2C), 124.2 (d), 123.4 (d), 121.0 (s), 117.4 (s), 117.3 (d), 45.0 (t, 2C).

dx.doi.org/10.1021/jm300505h | *J. Med. Chem.* 2012, 55, 5044−5060

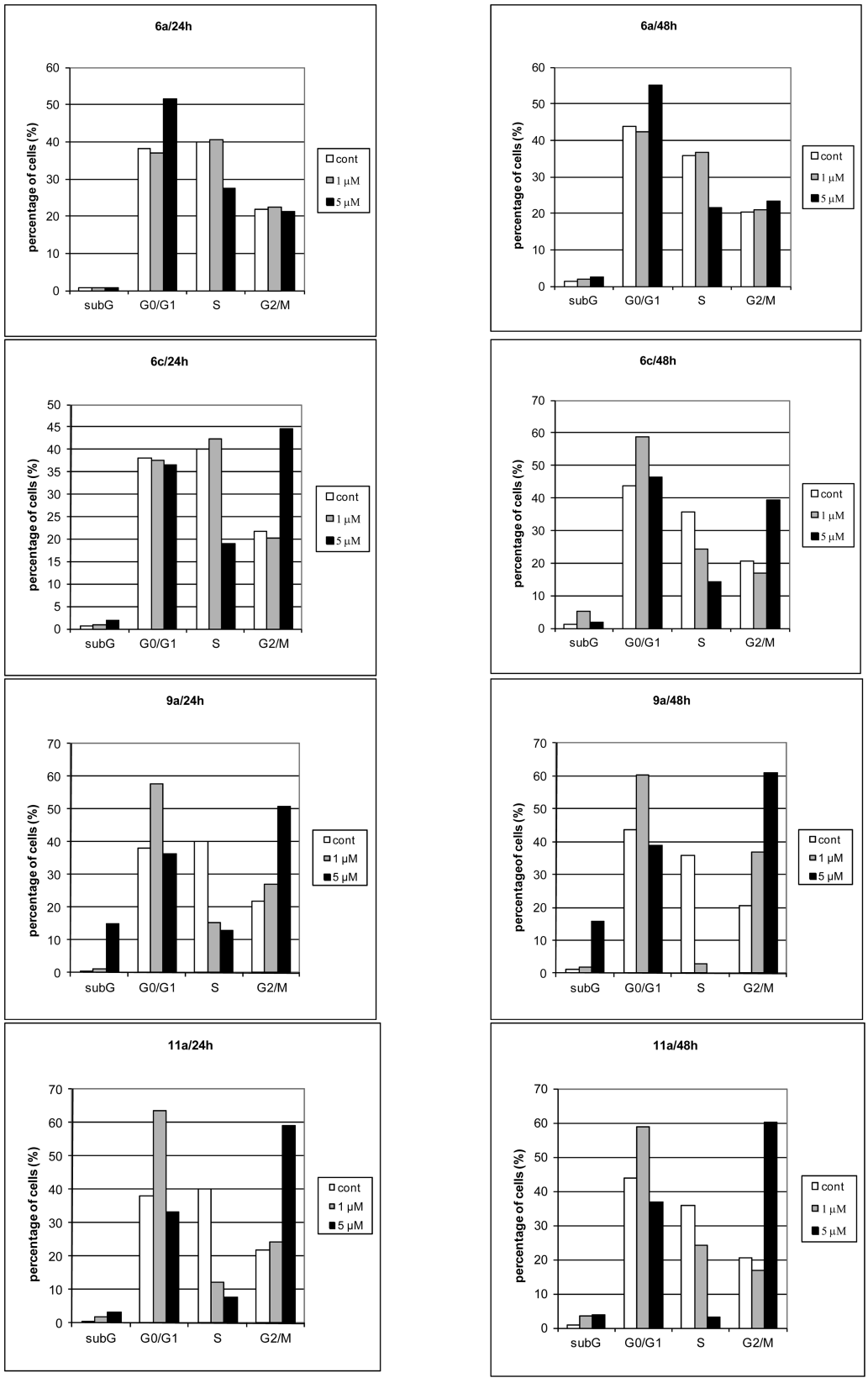

Figure 15. Effects of compound **6a**, **6c**, **9a**, and **11a** at 1 and 5 μM on the cell cycle distribution of HCT116 cells after the 24 and 48 h treatments. The histograms represent the percentages of cells in the respective cell cycle phase (G1, S, and G2/M), along with the percentage of cells in the subG1 (dead cells) obtained by flow cytometry.

2,9-(2-Diimidazolinyl)-6-oxo-5,6-dihydro[1]benzothieno-[2,3-*c*]quinolin-6-one Hydrochloride (9c). A solution of **6c** (0.10 g, 0.20 mmol) in water (75 mL) was irradiated for 1.5 h, and 0.03 g (32%) of light brown solid was obtained, mp >285 °C. IR ν/cm^{-1}:

dx.doi.org/10.1021/jm300505h | *J. Med. Chem.* 2012, 55, 5044−5060

3127, 2973, 1654, 1598. ^{1}H NMR (DMSO-d_6) (δ ppm): 12.77 (bs, 1H, $NH_{quinolone}$), 10.90 (bs, 4H, $NH_{amidine}$), 9.49 (d, 1H, J = 8.6 Hz, H_{arom}), 9.17 (s, 1H, H_{arom}), 8.94 (s, 1H, H_{arom}), 8.30 (d, 1H, J = 8.3 Hz, H_{arom}), 8.18 (d, 1H, J = 8.6 Hz, H_{arom}), 7.79 (d, 1H, J = 8.6 Hz, H_{arom}), 4.10 (d, 8H, J = 4.0 Hz, $CH_{2imidazolyl}$). ^{13}C NMR (DMSO-d_6) (δ ppm): 164.9 (s), 164.8 (s), 158.1 (s), 142.2 (s), 141.5 (s), 135.2 (s), 129.3 (d), 127.8 (d), 125.6 (d), 125.0 (d), 121.9 (d), 121.5 (s), 118.1 (d), 117.6 (s), 117.4 (s), 116.8 (s), 45.1 (t, 2C), 44.9 (t, 2C).

2-(2-Imidazolinyl)-5-methyl-6-oxo-5,6-dihydro[1]-benzothieno[2,3-*c*]quinolin-6-one Hydrocloride (11a). For the synthesis of **11a** was applied the method described for the compounds **6a**−**c**. A mixture of compound **10a** (0.15 g, 0.52 mmol) in dry ethanol (20 mL) was saturated with HCl gas and stirred until the nitrile band disappeared. The crude imidate was filtered off and was immediately suspended in absolute ethanol (20 mL). Ethylenediamine (0.11 mL, 1.63 mmol) was added. The mixture was stirred at reflux for 24 h, and 0.11 g (56%) of white solid was obtained, mp >285 °C. IR ν/cm^{-1}: 3210, 3101, 2973, 1649, 1618. ^{1}H NMR (DMSO-d_6) (δ ppm): 11.21 (bs, 2H, $NH_{amidine}$), 9.27−9.23 (m, 1H, H_{arom}), 9.18 (s, 1H, H_{arom}), 8.41−8.29 (m, 2H, H_{arom}), 8.04−8.00 (m, 1H, H_{arom}), 7.76−7.72 (m, 2H, H_{arom}), 4.09 (s, 3H, CH_3), 3.87 (s, 4H, $CH_{2imidazolyl}$). ^{13}C NMR (DMSO-d_6) (δ ppm): 164.6 (s), 158.0 (s), 142.6 (s), 141.9 (s), 135.2 (s), 134.5 (s), 129.3 (d), 128.4 (d), 127.3 (d), 126.6 (d), 124.9 (d), 124.5 (d), 118.7 (s), 117.8 (d), 116.7 (s), 44.9 (t, 2C), 30.8 (q).

Antitumor Evaluation Assay. The experiments were carried out on five human cell lines, which are derived from four cancer types. The following cell lines were used: SW620 and HCT116 (colon carcinoma), H460 (lung carcinoma), MCF-7 (breast carcinoma), and MOLT-4 (T-lymphoblast leukemia). MCF-7, SW620, HCT116, and H460 cells were cultured as monolayers and maintained in Dulbecco's modified Eagle's medium (DMEM), while MOLT-4 cells were cultured in suspension in RPMI medium, both supplemented with 10% fetal bovine serum (FBS), 2 mM L-glutamine, 100 U/mL penicillin, and 100 μg/mL streptomycin in a humidified atmosphere with 5% CO_2 at 37 °C.

The growth inhibition activity was assessed as described previously.[7−9,11,13,14] The panel cell lines were inoculated onto a series of standard 96-well microtiter plates on day 0 at 1×10^4 to 3×10^4 cells/mL, depending on the doubling times of a specific cell line. Test agents were then added in 10-fold dilutions (10^{-8}−10^{-4} M) and incubated for a further 72 h. Working dilutions were freshly prepared on the day of testing. After 72 h of incubation the cell growth rate was evaluated by performing the MTT assay, which detects dehydrogenise activity in viable cells. The absorbance (OD, optical density) was measured on a microplate reader at 570 nm. The absorbance is directly proportional to the number of living, metabolically active cells. The percentage of growth (PG) of the cell lines was calculated according to one of the following two expressions:

If (mean OD_{test} − mean OD_{tzero}) ≥ 0, then PG = 100 × (mean OD_{test} − mean OD_{tzero})/(mean OD_{ctrl} − meanOD_{tzero}). If (mean OD_{test} − mean OD_{tzero}) < 0, then PG = 100 × (mean OD_{test} − mean OD_{tzero})/OD_{tzero}, where the mean OD_{tzero} is the average of optical density measurements before exposure of cells to the test compound, the mean OD_{test} is the average of optical density measurements after the desired period of time, and the mean OD_{ctrl} is the average of optical density measurements after the desired period of time with no exposure of cells to the test compound.

Each test was performed in quadruplicate in at least two individual experiments. The results are expressed as IC_{50}, which is the concentration necessary for 50% of inhibition. The IC_{50} values for each compound are calculated from concentration−response curves using linear regression analysis by fitting the test concentrations that give PG values above and below the reference value (i.e., 50%). If, however, for a given cell line all of the tested concentrations produce PGs exceeding the respective reference level of effect (e.g., PG value of 50), then the highest tested concentration is assigned as the default value, which is preceded by a ">" sign. Each result is a mean value of three separate experiments.

Computational Analysis. The 3D-derived QSAR models were derived using the Volsurf+ program[17] generated molecular descriptors and the experimentally determined antitumor activities against MCF-7, SW620, HCT116, H460, and MOLT-4 cell lines. From the 23 synthesized compounds whose antitumor activities are presented in this paper, 20 of them were used for building the 3D-derived QSAR models. Besides, the 3D QSAR models were built considering only 17 (very) active compounds as well as a large set of 30 compounds, 20 from this publication and 10 from previous publications. Compounds **5a** and **9c** were shown to be outliers in all models and therefore were excluded from the data set. Compound **19** was synthesized and analyzed afterward and was used for the external validation of the derived models. Negative logarithmic values of concentrations that cause 50% growth inhibition of the cell lines (pIC_{50}) were used as a measure of biological activity in the 3D-derived QSAR models. For the poorly active compounds whose IC_{50} values were not explicitly measured but just estimated as >10 or ≥10, pIC_{50} was set to 4.301.

For each compound, the 3D structure was generated using the VolSurf+ program[17] and molecular interaction fields (MIFs) were calculated by the program GRID.[19] Grid spacing was set to 0.5 Å, and the following probes were used: H2O (the water molecule), O (sp^2 carbonyl oxygen atom), N1 (neutral NH group (e.g., amide)), and DRY (the hydrophobic probe). From the MIFs, VolSurf+ derived a series of 128 descriptors (independent of molecular alignment) that refer to molecular size and shape, to hydrophilic and hydrophobic regions and to the balance between them, to the "charge state", to lipophilicity, to molecular diffusion, to log P, to log D, to the presence/distribution of pharmacophoric groups, and to some other relevant ADME properties. The definition of all 128 VolSurf+ descriptors is given in the VolSurf+ manual. The 3D-derived QSAR models were derived for the raw data (models labeled as **B**, **D**, and **F**) as well as for the autoscaled ones (models labeled as **A**, **C**, and **E**). By the autoscaling pretreatment, every variable is the mean centered and scaled to give unit variance. Models **A**, **B**, **C**, and **D** were derived for compounds from the present study, the first two for the 20-object data set and the last two for the 17-objects data set. Models **E** and **F** were derived for 30-object data set comprising 20 compounds from the present study and 10 compounds from previous studies.[7,9] Models for different cel lines are distinguished by numbers **1**−**5** (MCF-7, HCT116, SW620, H460, MOLT-4). The 3D-derived QSAR models, i.e., the relationship between the 3D structure-based molecular descriptors and measured antitumor activity, were determined using the partial least square (PLS) analysis. The number of significant latent variables (nLV) and quality of the models were determined using the leave-one-out (LOO) cross-validation procedures. Standard deviation of error of calculation (SDEC) and standard deviation of error of prediction (SDEP) were calculated for each model.

In order to identify the descriptors with the highest (positive or negative) impact on biological activity of the compounds, PLS coefficients were analyzed for the 3D-derived QSAR models built using autoscaling (models **1A**, **2A**, **3A**, **4A**) pretreatment.

Principal component analysis (PCA) was performed in order to determine the distribution of the compounds in the space of the molecular descriptors and with an attempt to find an explanation for the outliers **5a** and **9c**. Usefulness of PCA in 3D-derived QSAR analysis has already been proved in several cases.[10,20,21]

Spectroscopic Evaluation of DNA Binding. *UV/Visible Spectrometry and DNA Melting Temperature Studies.* CT-DNA and double-stranded poly(dAdT)$_2$ oligonucleotide (Sigma Aldrich, France) were dissolved in water and dyalized overnight prior to use. The analyzed compounds were prepared as 10 mM stock solutions in DMSO, aliquoted, and stored at −20 °C and then freshly diluted in the appropriate aqueous buffer.

The various compounds were prepared at 20 μM in 1 mL of BPE buffer (6 mM Na_2HPO_4, 2 mM NaH_2PO_4, 1 mM EDTA, pH 7.1) in the presence or absence of increasing concentrations of CT-DNA or poly(dAdT)$_2$ (from 10 to 100 μM with 10 μM steps and then from 100 to 200 μM with steps of 20 μM of base pairs). The UV/visible spectra were recorded from 230 to 430 nm in a quartz cuvette of 10 mm path length using an Uvikon XL spectrophotometer and referenced against a cuvette containing DNA at identical concentration. The T_m values were obtained from the midpoint of the

hyperchromic transition obtained from first-derivative plots. The variation of melting temperature (ΔT_m) was measured by subtracting the melting temperature measurement of 20 μM CT-DNA or poly(dAdT)$_2$ incubated alone (control T_m) from that obtained with DNA incubated with increasing concentrations of the various tested compounds (drug/base pair ratio of 0.01−0.5) in 1 mL of BPE buffer ($\Delta T_m = T_{m[Drug+DNA]} - T_{m[DNA\ alone]}$). The absorbency of DNA was measured at 260 nm in quartz cells using a Uvikon 943 spectrophotometer thermostated with a Neslab RTE111 cryostat every minute over a range of 20−100 °C with an increment of 1 °C per min, and T_m values were deduced from the midpoint of the hyperchromic transition.

Circular Dichroism. To evaluate the orientation of the drug relative to the helicity of the DNA, the various drugs (50 μM) were incubated with or without (control) a fixed or increasing concentration of CT-DNA or poly(dAdT)$_2$ (from 1 to 200 μM) in BPE or BPE supplemented with 10 or 100 mM NaCl as specified in the figure captions. The CD spectra were collected in a quartz cell of 10 mm path length from 480 to 230 nm using a J-810 Jasco spectropolarimeter at a controlled temperature of 20 °C fixed by a PTC-424S/L Peltier type cell changer (Jasco) essentially as described previously.[22]

Biochemical Approaches for DNA Binding. *Radiolabeled DNA Fragments.* The 117 and 265 bp *Eco*RI and *Pvu*II DNA fragments were obtained from double digestion of the pBluscript plasmid (Stratagene, La Jolla, CA) using *Eco*RI (two sites) and *Pvu*II (1 site) restriction enzymes for 1 h in their respective buffers. The generated DNA fragment was 3′-end labeled at the generated 3′ available termini of the *Eco*RI cleaved sites upon addition of α-[^{32}P]dATP (3000 Ci/mmol, PerkinElmer, France) using Klenow enzyme for 30 min at 37 °C. After separation of the two fragments of interest from the plasmid remnant on a 6% native polyacrylamide gel in TBE buffer (89 mM Tris base, 89 mM boric acid, 2.5 mM Na_2 EDTA, pH 8.3), the portions of the gel containing the 117 and 265 bp radiolabeled DNA fragments were localized using a Molecular Dynamics STORM 860 and cut off from the gel, crushed, and dialyzed overnight. The eluted radioactive materials were filtered through a 0.22 μm membrane (Millipore). DNA fragments were finally ethanol-precipitated, dried, and dissolved in an appropriate amount of Milli-Q water.

DNase I Footprinting. DNase I footprinting experiments were performed essentially as previously described.[23] Increasing concentrations of the various compounds were incubated with the 265-bp radiolabeled DNA fragment for 15 min at 37 °C to ensure equilibrium prior to DNA digestion upon addition of DNase I (final concentration, 0.002 unit/mL) in reaction buffer (20 mM NaCl, 2 mM $MgCl_2$, 2 mM $MnCl_2$, pH 7.3). After mild digestion (4 min), the reaction was stopped by freeze-drying, lyophilization, and subsequent dissolution in 4 μL of denaturing loading buffer (80% formamide solution containing tracking dyes) prior to the mixture being heated at 90 °C for 4 min and chilled on ice for another 4 min. DNA cleavage products were resolved under polyacrylamide electrophoresis in denaturing conditions (0.35 mm thick, 8% polyacrylamide containing 8 M urea) for 90 min at 65 W in TBE buffer. Gels were finally soaked in 10% acetic acid, transferred to Whatman 3 MM paper, and dried under vacuum at 80 °C. After an exposition of the gels to storage screen for the appropriate delay at room temperature, the results were collected using a Molecular Dynamics STORM 860. Each base was localized from comparison with the bands from guanines sequencing standard (G-track) classically obtained using dimethyl sulfate (DMS) and piperidine treatment of the same DNA fragment.

Topoisomerase I Mediated DNA Relaxation and Topoisomerases Cleavage Assays. Topoisomerase I mediated DNA relaxation experiments were performed as previously described.[15] Graded concentrations of the tested compounds were incubated in the presence of supercoiled pUC19 plasmid DNA prior to the addition of 4 units of human topoisomerase I (Topogen, U.S.) at 37 °C for 45 min in relaxation buffer. The reactions were stopped upon addition of SDS (0.25%) and proteinase K (250 μg/mL) for a 30 min incubation at 50 °C. After addition of electrophoresis dye mixture, the DNA forms were separated on a 1% agarose gel without ethidium bromide for 2 h at 120 V in TBE buffer. Gels were then stained in a bath containing ethidium bromide before they were washed and photographed under UV light.

Topoisomerase I DNA cleavage assays were performed in the same condition exept that the samples were loaded on a 1% agarose gel prepared with ethidium bromide and that camptothecin (CPT, 20 μM) was used as a control for topoisomerase I poisoning effect.

In order to localize potential cleavage sites induced by topoisomerase I poisoning or suppressor activities, the reaction was conducted using the 3′-end-labeled 117 base pairs DNA fragment as already published[24] in the absence or presence of 20 μM CPT, respectively.

Topoisomerase II DNA cleavage assays were performed essentially as described,[16] with etoposide as a positive control for the Topo II poisoning effect.

Cell Cycle Analysis. Tumor cells (2×10^5) were seeded per well into a six-well plate. After 24 h the tested compounds were added at various concentrations (as shown in the Results and Discussion). After the desired length of time, the attached cells were trypsinized, combined with floating cells, washed with phosphate buffer saline (PBS), fixed with 70% ethanol, and stored at −20 °C. Immediately before the analysis, the cells were washed with PBS and stained with 50 μg/mL propidium iodide (PI) with the addition of 0.2 μg/μL RNase A. The stained cells were then analyzed with Becton Dickinson FACScalibur (Becton Dickenson) flow cytometer (20 000 counts were measured). The percentage of the cells in each cell cycle phase was determined using the ModFit LT software (Verity Software House) based on the DNA histograms. The tests were performed in duplicate and repeated at least twice.

■ ASSOCIATED CONTENT

Ⓢ Supporting Information

Experimental details, spectroscopic data, and elemental analysis results for compounds **2a−e**, **3a−e**, **4a−e**, **5a−e**, **7a−e**, **8a−c**, **10a**, **10b**, **11b**, **14−19**; elemental analysis results for **6a−c**, **9a−c**, and **11a**; antitumor activity of the compounds from the previous publications (**S1−10**); statistical properties of the 3D-derived QSAR models obtained using only the compounds analyzed in the present study; PCA scores plot derived for 30-data set; figures with predicted vs experimental antitumor activity for models **1A**, **1B**, **3A**, **3B**, **4A**, and **4B**; PLS coefficients for models **1A**, **2A**, **3A**, **4A**, **1C**, and **3C**; products of the descriptor average values and the associated PLS coefficients for models **1B**, **2B**, **3B**, and **4B**; and the topoisomerase I poisoning of the various compound using the 3′-end radiolabeled 117bp DNA fragment. This material is available free of charge via the Internet at http://pubs.acs.org.

■ AUTHOR INFORMATION

Corresponding Author

*For S.T.: phone, ++38514571251; fax, ++39514680245; e-mail, sanja.tomic@irb.hr. For G.K.-Z.: phone, ++38514597215; fax, ++39514597224; e-mail, gzamola@fkit.hr.

Present Address

[#]Center for Neuroscience and Cell Biology, Department of Zoology, University of Coimbra, 3004-517 Coimbra, Portugal.

Notes

The authors declare no competing financial interest.

■ ACKNOWLEDGMENTS

We greatly appreciate the financial support of the Croatian Ministry of Science Education and Sports (Projects 125-0982464-1356, 098-1191344-2860, 098-0982464-2514) and the bilateral Hubert Curien partnership between Croatian and French institutions (Cogito program) as the Egide Project No. 24765PH. The authors thank the Association Laurette Fugain,

the Ligue Nationale Contre le Cancer (Comité du Pas-de Calais, Septentrion), the Fonds Européen de Développement Régional (FEDER, European Community), and the Région Nord-Pas de Calais for grants (M-H.D.-C.), the Université de Lille-2 together with the Région Nord-Pas de Calais for a Ph.D. fellowship to R.N., and the Institut pour la Recherche sur le Cancer de Lille (IRCL) for technical expertise (S.D.), as well as the IMPRT-IFR114 for access to the Strom 860 equipment.

REFERENCES

(1) Letafat, B.; Emami, S.; Mohammadhosseini, N.; Faramarzi, M. A.; Samadi, N.; Shafiee, A.; Foroumadi, A. Synthesis and Antibacterial Activity of New *N*-[2-(thiophen-3-yl)ethyl]piperazinyl Quinolones. *Chem. Pharm. Bull.* **2007**, *55*, 894−898.

(2) Wang, S. W.; Pan, S. L.; Huang, Y. C.; Guh, J. H.; Chiang, P. C.; Huang, D. Y.; Kuo, S. C.; Lee, K. H.; Teng, C. M. CHM-1, a Novel Synthetic Quinolone with Potent and Selective Antimitotic Antitumor Activity against Human Hepatocellular Carcinoma in Vitro and in Vivo. *Mol. Cancer Ther.* **2008**, *7*, 350−360.

(3) Hoang, H.; LaBarbera, D. V.; Mohammed, K. A.; Ireland, C. M.; Skibo, E. B. Synthesis and Biological Evaluation of Imidazoquinoxalinones, Imidazole Analogues of Pyrrolo-iminoquinone Marine Natural Products. *J. Med. Chem.* **2007**, *50*, 4561−4571.

(4) Chen, M. H.; Fitzgerald, P.; Singh, S. B.; O'Neill, E. A.; Schwartz, C. D.; Thompson, C. M.; O'Keefe, S. J.; Zaller, D. M.; Doherty, J. B. Synthesis and Biological Activity of Quinolinone and Dihydroquinolinone p38 MAP Kinase Inhibitors. *Bioorg. Med. Chem. Lett.* **2008**, *18*, 2222−2226.

(5) Dogan Koruznjak, J.; Slade, N.; Zamola, B.; Pavelić, K.; Karminski-Zamola, G. Synthesis, Photochemical Synthesis and Antitumor Evaluation of Novel Derivatives of Thieno[3′,2′:4,5]thieno-[2,3-*c*]quinolones. *Chem. Pharm. Bull.* **2002**, *50*, 656−660.

(6) Dogan Koruznjak, J.; Grdiša, M.; Slade, N.; Zamola, B.; Pavelić, K.; Karminski-Zamola, G. Novel Derivatives of Benzo[*b*]thieno[2,3-*c*]quinolones: Synthesis, Photochemical Synthesis and Antitumor Evaluation. *J. Med. Chem.* **2003**, *45*, 4516−4524.

(7) Jarak, I.; Kralj, M.; Šuman, L.; Pavlović, G.; Dogan, J.; Piantanida, I.; Žinić, M.; Pavelić, K.; Karminski-Zamola, G. Novel Cyano- and *N*-Isopropylamidino-Substituted Derivatives of Benzo[*b*]thiophene- 2-carboxanilides and Benzo[b]thieno[2,3-*c*]quinolones: Synthesis, Photochemical Synthesis, Crystal Structure Determination and Antitumor Evaluation. Part 2. *J. Med. Chem.* **2005**, *48*, 2346−2360.

(8) Jarak, I.; Kralj, M.; Piantanida, I.; Šuman, L.; Žinić, M.; Pavelić, K.; Karminski-Zamola, G. Novel Cyano- and Amidino-Substituted Derivatives of Thieno[2, 3-*b*]- and Thieno[3, 2-*b*]thiophene-2-carboxanilides and Thieno[3′,2′:4,5]thieno- and Thieno[2′,3′:4, 5]-thieno[2,3-*c*]quinolones: Synthesis, Photochemical Synthesis, DNA Binding and Antitumor Evaluation. *Bioorg. Med. Chem.* **2006**, *14*, 2859−2868.

(9) Ester, K.; Hranjec, M.; Piantanida, I.; Ćaleta, I.; Jarak, I.; Pavelic, K.; Kralj, M.; Karminski-Zamola, G. Novel Derivatives of Pyridylbenzo[*b*]thiophene-2-carboxamides and Benzo[*b*]thieno[2,3-*c*]naphthyridin-2-ones: Minor Structural Variations Provoke Major Differences of Antitumor Action Mechanisms. *J. Med. Chem.* **2009**, *52*, 2482−2492.

(10) Bertoša, B.; Aleksić, M.; Karminiski-Zamola, G.; Tomić, S. QSAR Analysis of Antitumor Active Amides and Quinolones from Thiophene Series. *Int. J. Pharm.* **2010**, *394*, 106−114.

(11) Čaleta, I.; Kralj, M.; Marjanović, M.; Bertoša, B.; Tomić, S.; Pavlović, G.; Pavelć, K.; Karminski-Zamola, G. Novel Cyano- and Amidinobenzothiazole Derivatives: Synthesis, Antitumor Evaluation, and X-ray and Quantitative Structure−Activity Relationship (QSAR) Analysis. *J. Med. Chem.* **2009**, *52*, 1744−1756.

(12) Bertoša, B.; Kojić-Prodić, B.; Ramek, M.; Piperaki, S.; Tsantili-Kakoulidou, A.; Wade, R.; Tomić, S. A New Approach To Predict the Biological Activity of Molecules Based on Similarity of Their Interaction Fields and the log*P* and log*D* Values: Application to Auxins. *J. Chem. Inf. Model.* **2003**, *43*, 1532−1541.

(13) Hranjec, M.; Kralj, M.; Piantanida, I.; Sedic, M.; Suman, L.; Pavelić, K.; Karminski-Zamola, G. Novel Cyano- And Amidino-Substituted Derivatives of Styryl-2-benzimidazoles and Benzimidazo-[1,2-*a*]quinolines. Synthesis, Photochemical Synthesis, DNA Binding and Antitumor Evaluation, Part 3. *J. Med. Chem.* **2007**, *50*, 5696−5711.

(14) Hranjec, M.; Piantanida, I.; Kralj, M.; Suman, L.; Pavelic, K.; Karminski-Zamola, G. Novel Amidino-Substituted Thienyl- and Furylvinyl-benzimidazole Derivatives and Their Photochemical Conversion into Corresponding Diaza-cyclopenta[*c*]fluorenes. Synthesis, Interactions with DNA and RNA and Antitumor Evaluation. Part 4. *J. Med. Chem.* **2008**, *51*, 4899−4910.

(15) Peixoto, P.; Bailly, C.; David-Cordonnier, M.-H. Topoisomerase I-Mediated DNA Relaxation as a Tool To Study Intercalation of Small Molecules into Supercoiled DNA. *Methods Mol. Biol.* **2010**, *613*, 235−256.

(16) Serbetçi, T.; Depauw, S.; Prado, S.; Porée, F.-X.; Hildebrand, M.-P.; David-Cordonnier, M.-H; Michel, S; Tillequin, F. Benzo[*c*]-[1,7] and [1,8]phenanthrolines Substituted with an Aminoalkyl Chain: Synthesis and Evaluation of the Cytotoxicity and the Topoisomerase 1 Inhibition. *Eur. J. Med. Chem.* **2010**, *45*, 2547−2558.

(17) Cruciani, G.; Crivori, P.; Carrupt, P.-A.; Testa, B. Molecular Fields in Quantitative Structure−Permeation Relationships: The VolSurf Approach. *J. Mol. Struct.: THEOCHEM* **2000**, *503*, 17−30.

(18) Cruciani, G.; Pastor, M.; Guba, W. VolSurf: A New Tool for Pharmacokinetic Optimization of Lead Compounds. *Eur. J. Pharm. Sci.* **2000**, *11*, S29−S39.

(19) Goodford, P. J. A Computational Procedure for Determining Energetically Favorable Binding Sites on Biologically Important Macromolecules. *J. Med. Chem.* **1985**, *28*, 849−857.

(20) Tomić, S.; Bertoša, B.; Kojić-Prodić, B.; Kolosvary, I. Stereoselectivity of *Burkholderia cepacia* Lipase towards Secondary Alcohols: Molecular Modelling and 3D QSAR Approach. *Tetrahedron: Asymmetry* **2004**, *15*, 1163−1172.

(21) Tomić, S.; Bertoša, B.; Wang, T.; Wade, R. C. COMBINE Analysis of the Specificity of Binding of Ras Proteins to Their Effectors. *Proteins: Struct., Funct., Bioinf.* **2007**, *67* (2), 435−447.

(22) Lemster, T.; Pindur, U.; Depauw, S.; Lenglet, G.; Dassi, C.; David-Cordonnier, M.-H. Photochemical Electrocyclisation of 3-Vinylindoles to Pyrido[2,3-*a*]-, Pyrido[4,3-*a*]- and Thieno[2,3-*a*]-carbazoles: Design, Synthesis, DNA-Binding and Antitumor Cell Cytotoxicity. *Eur. J. Med. Chem.* **2009**, *44*, 3235−3252.

(23) Peixoto, P.; Liu, Y.; Depauw, S.; Hildebrand, M.-P.; Boykin, D. W.; Bailly, C.; Wilson, W. D.; David-Cordonnier, M.-H. Direct Inhibition of the DNA Binding Activity of POU Transcription Factors Pit-1 and Brn-3 by Selective Binding of a Phenyl-furan-benzimidazole Dication. *Nucleic Acids Res.* **2008**, *36*, 3341−3353.

(24) Genès, C.; Lenglet, G.; Depauw, S.; Nhili, R.; Prado, S.; David-Cordonnier, M.-H.; Michel, S.; Tillequin, F.; Porée, F.-H. Synthesis and Biological Evaluation of N-Substituted Benzo[*c*]phenanthrolines and Benzo[*c*]phenanthrolinones as Antiproliferative Agents. *Eur. J. Med. Chem.* **2011**, *46*, 2117−2131.